IEEE Access
Multidisciplinary ⋮ Rapid Review ⋮ Open Access Journal

Received 1 May 2023, accepted 22 May 2023, date of publication 24 May 2023, date of current version 1 June 2023.

Digital Object Identifier 10.1109/ACCESS.2023.3279820

RESEARCH ARTICLE

Nature-Inspired Intelligent Synthesis of a Spherical Mechanism for Passive Ankle Rehabilitation Using Differential Evolution

LUIS ERNESTO VALENCIA-SEGURA[1,2], MIGUEL GABRIEL VILLARREAL-CERVANTES[1], (Member, IEEE), LEONEL GERMÁN CORONA-RAMÍREZ[2], FRANCISCO CUENCA-JIMÉNEZ[3], AND JOSÉ SAÚL MUÑZ-REINA[1]

[1]Postgraduate Department, Mecatronic Section, CIDETEC, Instituto Politécnico Nacional, Mexico City 07700, Mexico
[2]UPIITA, Instituto Politécnico Nacional, Mexico City 07340, Mexico
[3]Engineering Faculty, Universidad Nacional Autónoma de México, Mexico City 04510, Mexico

Corresponding author: Miguel Gabriel Villarreal-Cervantes (mvillarrealc@ipn.mx)

This work was supported in part by the Secretaría de Investigación y Posgrado (SIP) of the Instituto Politécnico Nacional (IPN) under Project 20180196, Project 20220255, Project 20221407, Project 20210314, and Project 20230320. The work of Luis Ernesto Valencia-Segura was supported by the Mexican Consejo Nacional de Ciencia y Tecnología (CONACyT) through Centro de Innovación y Desarrollo Tecnològico en Cómputo, Instituto Politécnico Nacional (CIDETEC-IPN).

ABSTRACT The ankle rehabilitation in certain injuries requires passive movements to aid in the prompt recovery of ankle movement. In the last years, parallel ankle rehabilitation robots with multiple degrees of freedom have been the most studied for providing such movements in a controlled way. Nevertheless, the high cost does not make it viable for home healthcare. Then, this paper presents an optimization approach where a spherical mechanism of one-degree-of-freedom is proposed as a low-cost ankle rehabilitation device to provide the passive rehabilitation exercise for plantar flexion/dorsiflexion and adduction/abduction ankle movements. The approach is formulated as a mono-objective constraint optimization problem where the relative motion angle of the mechanism, the Grashof criterion, the force transmission, and the rehabilitation routine are included. The link lengths of the mechanism parameterized in Cartesian coordinates are found by the two most representative differential evolution variants. The statistical analysis of optimizers indicates that the $DE/rand/1/bin$ finds, on average, more promising solutions through algorithm executions than the $DE/best/1/bin$. The numerical simulation results and the motion simulation of the CAD model illustrate the obtained ankle rehabilitation mechanism, indicating that the percentage error between the desired rehabilitation path and the curve generated by the coupler point of the mechanism is in the interval [0.036, 0.437]%. Manufacturing the ankle rehabilitation mechanism with a 3D printer validates the optimization approach and verifies the resulting mechanism.

INDEX TERMS Mechanism synthesis, spherical four-bar mechanism, optimization, differential evolution.

I. INTRODUCTION

The ankle is the fundamental joint for balance, support, and propulsion of the human body. Musculoskeletal and neurological injuries alter the ankle movement [1]. Obesity can also produce musculoskeletal disorders, overloading the joints and reducing the range of ankle motion [2], [3]. The sprained ankle is the single most common injury with approximately 80% of ankle injuries in individuals with physical activities during sporting events, recreational activities, and occupational accidents [4], [5]. For instance, one in every ten thousand people suffers from inversion ankle sprains in sports every day [6], and approximately 5600 injuries per day

The associate editor coordinating the review of this manuscript and approving it for publication was Huaqing Li.

in United Kingdom [7]. This injury often causes a kind of disability.

The recovery of the ankle movement depends on the stimulation of the central nervous system and the motor system perception function. Then, physiotherapy plays an essential role in the recovery of the ankle motion [4]. Nevertheless, the therapists' long, repetitive, and intense rehabilitation process leads to inaccurate training in the rehabilitation movements and/or in the required training forces. Also, the limited therapist resources available in the institutions (hospitals, rehabilitation centers, etc.) can delay ankle injury treatment. So the return of patients to normal activities is prolonged for a longer time [4].

Hence, several robotic devices have been developed to replace traditional ankle rehabilitation training provided by therapists. Parallel robots for ankle rehabilitation, called parallel ankle rehabilitation robots (PARRs), are used for general ankle rehabilitation purposes [1], i.e., they can perform different rehabilitation routines. So, the potential of the rehabilitation robots is evidenced as an aid in developing ankle rehabilitation exercises to recover the lost range of motion and muscle strength.

Stewart parallel mechanism [8] is the pioneered configuration used in the PARRs by Rutgers University [9]. In order to reduce the coupling degree in its six Degree Of Freedom (DOF) that conducts to a hard controller, parallel mechanisms with fewer DOF have been used in the PARRs to simplify the robot model and, as a consequence, the control system. Some examples are the 3-DOF 3RSS/S parallel mechanism [10], the 2-DOF 3UPS/U parallel mechanism [11], the 3-SPS/SP parallel mechanism [12], where R, U, and S represents the revolute, universal and spherical joint, respectively.

Soft actuators like Pneumatic Muscles (PMs) and cables have been introduced in the PARRs to perform the full range of motion of the ankle and torque. PMs possess the advantage of better flexibility, lightweight, high power/mass ratio, and better human-robot interactions [13] with respect to the rigid actuators. Nevertheless, the PM-driven PARRs must have at least one PM more than the DOF [14]. Moreover, the control system must be more sophisticated because the tension in the PMs must be kept in the development of exercises, and the loss of its control (control system instability) might injure patients whether a deviation from the safe workspace occurs [15].

On the other hand, in the previous PARRs, the instantaneous centers of rotation of the PARRs (robot rotation axes) are just below the foot sole. As a consequence, the robot rotation axes present deviations from the ankle rotation axes causing unexpected movement and forces in the patients; hence, the patients might not reproduce the correct movements given by the therapist because of the repetitively changes of the sitting postures during the exercises or even, the patients might suffer secondary damage [16]. The design of PARRs that presents a stationary center of rotation coincident with the ankle center is one of the research directions in the state-of-the-art. For instance, the 3-DOF 2-UPS/RRR parallel mechanism is proposed in [17], the 2-DOF based on crank-slider mechanism in [18], the 3-DOF spherical RRR parallel mechanism in [19] based on a redesign of the Agile Eye Gosselin's robot [20], the generalized spherical parallel mechanism which considers 3-5 DOF is given in [16].

However, the high degree of freedom of the PARRs makes them less affordable to be wearable devices. This is because of the high weight due to the increment of actuators, the complexity in their use for programming the rehabilitation exercises due to they are robots for general purposes, and the high cost due to the increment of actuators which implies an advanced technology for controlling. Others researches have motivated the use of fewer DOF PARRs to perform two of the three kinds of ankle movements (plantarflexion/dorsiflexion, eversion/inversion, and adduction/abduction) [11], [21]. On the other hand, the complex movement of some parts of the human body can be reproduced by using mechanisms with one-degree-of-freedom without reducing the performance and functionality of the rehabilitation machine [22].

Nevertheless, it is well known that the mechanism's performance is highly dependent on its geometry. Therefore the dimensional synthesis plays a vital role in its design, and the way of stating the synthesis impacts the obtained design [23]. The mechanism synthesis is a complex, multimodal, constrained and large-scale design problem [24] that consists of determining the size and configuration of the mechanism to yield the required motion [25], [26]. Three main kinds of mechanism synthesis are considered in the literature: type synthesis, number synthesis, and dimensional synthesis. Furthermore, dimensional synthesis can be categorized into three classes: path generation, function generation, and motion generation (body guidance). This paper deals with the path generation dimensional synthesis problem where the link lengths are determined such that a point (Cartesian position) in the coupler link, called coupler point, must follow, as close as possible, a set of points (path).

Recent results from the authors of this work [23] indicate that handling in a different way kinematic synthesis optimization problem can aid in the search for solutions by the optimizer. In this direction, the development of the ankle rehabilitation device through a spherical mechanism with one-degree-of-freedom that performs the complex task of two kinds of ankle movements (ankle rehabilitation exercise), is the main objective of this work. So, in this paper, the relative motion angle approach for spherical mechanisms, the Grashof criterion, and the force transmission are incorporated in the formulation of the path generation-based dimensional synthesis where the link lengths are parameterized with Cartesian coordinates, and the passive rehabilitation exercise is considered in the optimization approach to make the ankle rehabilitation device. One of the benefits of using spherical mechanisms to make ankle rehabilitation routines is that the mechanism rotation axes coincide with the ankle rotation

allowing the correct movements without changes in the sitting postures.

On the other hand, finding the exact synthesis problem of the spherical mechanism with more than nine precision points leads to an overdetermined system of nonlinear equations in which the exact solution cannot reach [27]. Therefore, to solve the synthesis problem, numerical optimization is applied. The least-square optimization scheme has been applied to the path generation dimensional synthesis in [28], to the function generation dimensional synthesis in [29], and to the motion generation dimensional synthesis in [30] of spherical four-bar mechanisms. In the motion generation dimensional synthesis of spherical four-bar mechanisms, sequential quadratic programming (SQP) is employed in [31] to solve the mechanism synthesis problem handled with the aid of harmonic analysis.

One of the problems with using least-square optimization and the SQP algorithm to fulfill the first-order optimality condition (a set of overdetermined nonlinear equations) is the requirement of tedious and complicated processes to find a good initial condition and also the well-conditioned Jacobian matrix. Damping and continuation techniques are used in [28] to accelerate the iterative process' convergence rate while stabilizing the process. Another approach reported in [30] uses fuzzy identification and the numerical atlas method [32] of spherical four-bar mechanisms to find the initial condition to reduce the fixed step sizes in the numerical atlas database. This finds better solutions between the basic dimensions given in the atlas. Nevertheless, setting the initial conditions in those algorithms is an important issue in the convergence to the most promising solution because they converge to the solution near the initial one. Furthermore, the strong dependency on gradient information also requires satisfying the continuity of the performance function and constraints. Those issues make the implementation of such algorithms a challenge for practitioners. Given the limitation of gradient-based algorithms, which restrict their effectiveness in complex engineering optimization problems, nature-inspired intelligent synthesis has been applied to the mechanism synthesis problem because they do not depend on the problem features (linearity, continuity, data types, etc.), they are population-based techniques that are less susceptible to converging to local solutions, and hence, they do not depend on a rigorous procedure to set the initial condition.

Nature-inspired intelligent synthesis solves the synthesis of mechanisms by nature-inspired computing based on the principles of physics and biology. The nature-inspired computing [33] are search techniques inspired by natural phenomena such as physics, chemistry, and biology. They are commonly used for finding solutions to complex constrained optimization problems and so, those have been highly used in the mechanism synthesis problem.

Table 1 presents the synthesis of different mechanisms using nature-inspired computing. It is observed in the circle chart in Fig. 1 that the three most frequently used algorithms in the synthesis problem are those based on Differential Evolution (DE) [34], Genetic Algorithm (GA) [35], and Particle Swarm Optimization (PSO) [36]. The DE-based algorithms represent the most useful approach in this kind

TABLE 1. Researches in the kinematic synthesis problem using nature-inspired computing.

Study	Application of the synthesis problem	Used algorithms
[40]	Spherical mechanism	Differential Evolution (DE)
[41]	Four-bar mechanism	Genetic Algorithm (GA)
[42]	Four-bar and Stephenson's six-bar mechanisms Watt's six-bar mechanism	GA
[43]	Four-bar mechanism	GA
[44]	Hand robot mechanism	Pareto Optimum Evolutionary, Multiobjective Algorithm (POEMA)
[45]	Four-bar mechanism	DE
[46]	Six-bar mechanism	DE
[47]	Six-bar mechanism	DE
[48]	Four-bar mechanism	GA–Fuzzy Logic
[49]	Four-bar and Six-bar mechanisms	Malaga University Mechanism Synthesis Algorithm (MUMSA)
[50]	Four-bar mechanism	Imperialist Competitive Algorithm (ICA), GA DE, Particle Swarm Optimization (PSO)
[51]	Four-bar mechanism	GA, DE, PSO
[52]	Four-bar mechanism	Ant-Gradient (AG)
[53]	Four-bar mechanism	GA–DE
[54]	Six-bar mechanism	Cuckoo Search (CS)
[55]	Four-bar mechanism	Non-dominated Sorting Genetic Algorithm II (NSGA-II)
[56]	Four-bar mechanism	Modified Krill Herd (MKH)
[57]	Four-bar mechanism	Teaching-Learning-Based-Optimization (TLBO), GA, PSO
[58]	Four-bar mechanism	Hybrid Lagrange Interpolation DE (HLIDE)
[59]	Four-bar and Six-bar mechanisms	Hybridization DE with Generalized Reduced Gradient
[23]	Four-bar mechanism	DE
[60]	Four-bar mechanisms	CS, TLBO, DE, Auto-adaptive modified DE, MUMSA, Combined-Mutation DE (CMDE)
[24]	Four-bar mechanism	Repellency Evolutionary Algorithm (REA) Sine Cosine Algorithm (SCA), TLBO with Self Regulating PSO (SRPSO), Backtracking Search optimization Algorithm (BSA), Gray Wolf Optimizer (GWO), Krill Herd (KH), Whale Optimization Algorithm (WOA) Dynamic Group Strategy (DGSTLBO)
[61]	Four-bar mechanism	Hybrid-Combined DE-Jaya algorithm (HCDJ), CMDE, Ingeniería Mecánica Málaga (IMMa) Optimization Algorithm with Self-Adaptive Technique IOA^{s-at}, Jaya, GA, DE, PSO, MUMSA
[62]	Four-bar mechanism	Self-Adaptive Population size Teaching- Learning Based Optimization (SAP-TLBO), GWO, Artificial Bee Colony (ABC), TLBO, Real-Code Ant Colony Optimization (ACOR), Adaptive Differential Evolution with optional external archive (JADE), Jaya, SCA, Population-Based Incremental Learning (PBIL)
[63]	Four-bar mechanism	Adaptive Inertia Weight PSO (AIW-PSO)
[64]	Single-DOF linkage-type grasper	AIW-PSO, PSO, GA
[65]	Flexible slider crank mechanism	Ant Colony Optimization (ACO), ABC, ICA, GA, Simulating Annealing (SA), DE
[66]	Four-bar mechanism	Error Feedback Method (EFM), PSO, DE, TLBO
[67]	Four-bar mechanism	GA
[68]	Slider-crank mechanism	NSGSA-II, DE, TLBO, Modified PSO and Multi-objective PSO (MOPSO)
	1-DOF mechanism synthesis for different kind of rehabilitation	
[69]	Spherical parallel manipulator in prosthetic wrist	Multi-Objective Evolutionary Algorithm based on Decomposition (MOEA/D), MOPSO, NSGA-II
[70]	Six-bar mechanism in finger rehabilitation	MUMSA
[71]	Cam-linkage mechanism in gait rehabilitation	GA
[72]	Four-bar mechanism in gait rehabilitation and orthotic devices	PSO, TLBO
[73]	Eight-bar mechanism in lower limb rehabilitation	DE
[74]	Eight-bar, four-bar and cam-linkage mechanisms in lower limb rehabilitation	DE, PSO, MUMSA, GA
[75]	Eight-bar and four-bar mechanisms in lower limb rehabilitation	DE, PSO, MUMSA, GA DE with Neuronal Constraint-Handling
[76]	Six-bar mechanism	TLBO, Best–Worst Play (BWP)
[77]	Crank and rod slider mechanism	PSO
[78]	Double-spherical 6R mechanism	Firefly Algorithm

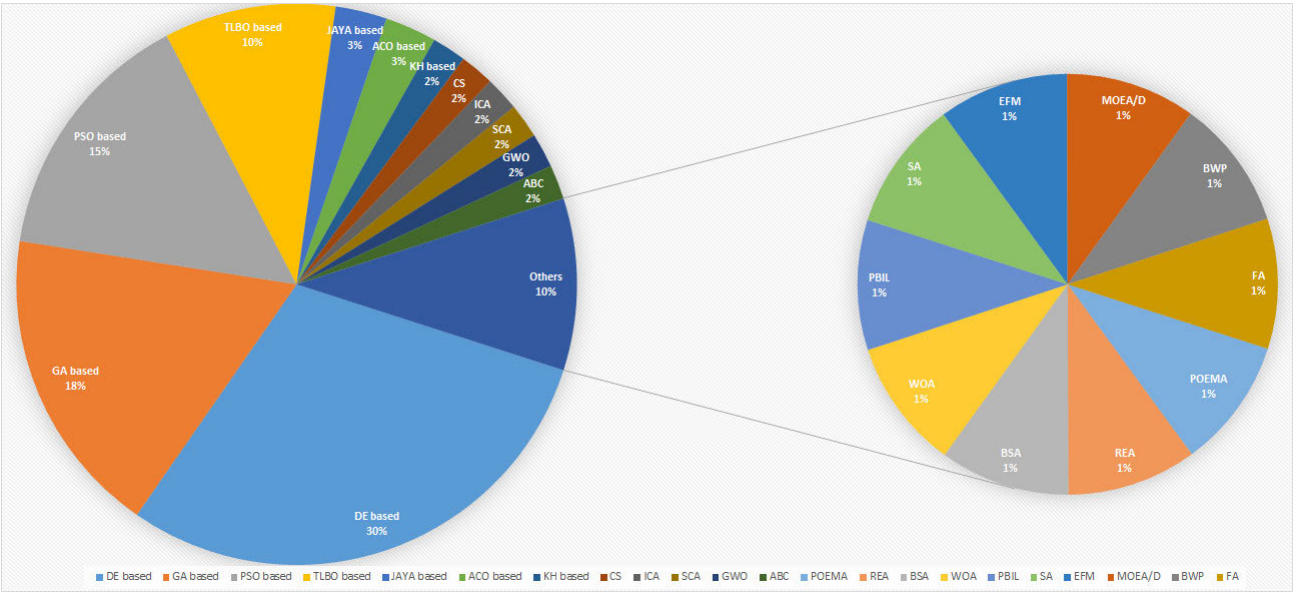

FIGURE 1. Circle chart of the different nature-inspired computing applied in the mechanism synthesis.

of problem and other real-world optimization problems [37], [38] because DE is a simple algorithm that, with straightforward adjustments to the DE coding, can produce an efficient search (accuracy, robustness, and speed) and an improved ability to solve problems than other algorithms inspired by other sources of inspiration. For instance, in the Congress of Evolutionary Computation competitions, DE based algorithms are the top three best-performing optimizers [39]. Then, this paper uses two different variants of the DE algorithm to solve the synthesis problem for the proposed 1-DOF spherical passive ankle rehabilitation mechanism.

A. CONTRIBUTIONS

The PARRs have been designed for developing different rehabilitation exercises with sophisticated control systems. Nevertheless, the high cost, the large volume, and complex control systems have led to providing other alternatives for making passive ankle rehabilitation. In particular, the spherical mechanism with one-degree-of-freedom is selected in this paper for making the passive ankle rehabilitation routine and is considered as option for ankle rehabilitation. Due to the complexity in the spherical mechanism design, the main aim of this work is the proposal of an optimization approach based on differential evolution for the design of the ankle rehabilitation device through this mechanism. In addition, this mechanism leads to a low-cost and lightweight design alternative for the rehabilitation device due to the reduction of actuators. The device obtained with this approach allows a particular routine within certain limits in the degree of freedom of ankle joint movement, which the routine can be previously set or depend on the anthropometric measurements of the population or a specific injury. So, different from the application of a robot to perform the rehabilitation routines, the presented proposal requires different mechanisms to provide different movements (rehabilitation routines) conforming to the rehabilitation training. A particular routine is set up as a study case, but the presented design approach is not limited to carrying out other different routines, i.e., the procedure developed in the following sections allows to design other devices for another particular routine.

On the other hand, the works in Table 1 requires the loop closure equations to determine the kinematic motion and the obtained parameters are the magnitude and direction of links. For instance, in [40], the closed-form expression of the output link angle is used to solve the spherical synthesis problem. The inclusion of this expression requires a high penalty on the optimization process when any non-zero number is divided by zero. Both the closed-form expression and the penalty functions reduce the ability of the algorithm to search for the whole design space. This leads to the requirement for modifications in the optimizer to find the most suitable solution, which is evidenced in [23]. In recent results of the authors of this work [23], the optimizers in the synthesis problem of the *planar* four-bar mechanism can significantly improve (without requiring algorithm modifications) the search for solutions by including the relative angle approach for producing kinematic motion and the link parameterization in terms of Cartesian coordinates. This results in a mechanism with better performance that directly impacts in the application. Unlike those works, in this work relative angle approach for providing the kinematic motion of the spherical mechanism is integrated into the path generation dimensional synthesis, where the link length parameterization with Cartesian coordinates and the passive rehabilitation exercise are also included to make the passive ankle rehabilitation device.

B. PAPER ORGANIZATION

The organization of this work is as follows. First, the kinematic analysis of the spherical mechanism using the relative angle method is presented in Section II. In Section III, the dimensional synthesis of the spherical mechanism for ankle rehabilitation is formally established as an optimization problem where the objective function, design variables, and constraints are presented. A brief explanation of two different differential evolution variants that solves the problem is described in Section IV. Fifth, the analysis and discussion of the obtained results with the DE variants are detailed in Section V. In addition, the obtained spherical mechanism design for ankle rehabilitation is validated through numerical simulations and also in experimentation with a physical prototype. Finally, the conclusions are drawn in Section VI.

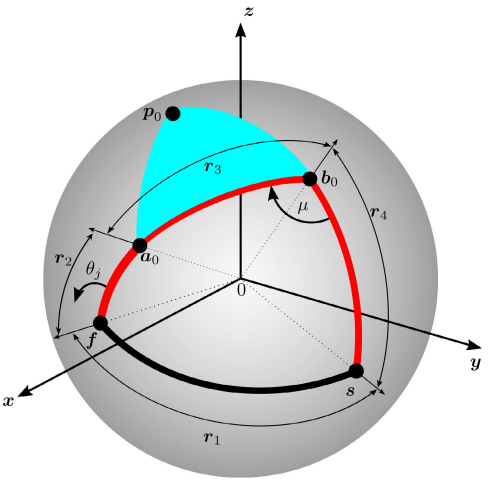

FIGURE 2. Initial position of the spherical four-bar mechanism.

II. KINEMATIC ANALYSIS OF THE SPHERICAL FOUR-BAR MECHANISM

The kinematic motion analysis of the spherical four-bar mechanism is obtained through the relative joint rotation angle method [79]. The spherical four-bar mechanism is shown in Fig. 2. The main feature of such mechanism is that all links are placed on the spherical surface with center in $\mathbf{0} = [0, 0, 0]^T$. The Cartesian coordinates or points of the link's tips with respect to the coordinate system $x - y - z$ are set as $\boldsymbol{a}_0 = [a_{0x}, a_{0y}, a_{0z}]^T$, $\boldsymbol{b}_0 = [b_{0x}, b_{0y}, b_{0z}]^T$, $\boldsymbol{f} = [f_x, f_y, f_z]^T$ and $\boldsymbol{s} = [s_x, s_y, s_z]^T$. Those points have revolute joints along the axis formed by the corresponding Cartesian coordinate and the sphere's center $\mathbf{0}$. Also, the Cartesian coordinate $\boldsymbol{p}_0 = [p_{0x}, p_{0y}, p_{0z}]^T$ represents the coupler point, and θ_j is the $j-th$ relative input angle of the crank link (formed by the points $\boldsymbol{a}_j$ and $\boldsymbol{f}$) around the unit vector $(\boldsymbol{f} - \mathbf{0})$. The relative reference of the angular displacement θ_j is the initial position of the spherical four-bar mechanism. This initial position contemplates the joint coordinates $\boldsymbol{a}_0, \boldsymbol{b}_0, \boldsymbol{f}, \boldsymbol{s}$ and $\boldsymbol{p}_0$.

The proposed spherical four-bar mechanism belongs to the surface of a sphere with unit radius (the links are normalized to unity), such that all points are on the same spherical surface. In the case that two points belong to the same rigid body, the geodesic distance [80] between them represents the link length. Then, the crank link length is represented by the geodesic distance $r_2 = cos^{-1}(\boldsymbol{f} \cdot \boldsymbol{a}_0)$, the length of the ground link is given by $r_1 = cos^{-1}(\boldsymbol{f} \cdot \boldsymbol{s})$, the coupler link length is provided by $r_3 = cos^{-1}(\boldsymbol{a}_0 \cdot \boldsymbol{b}_0)$ and the output link length is set as $r_4 = cos^{-1}(\boldsymbol{s} \cdot \boldsymbol{b}_0)$. In the real application, the links of the spherical mechanism must fit to the real size by scaling up the geodesic distances.

In the kinematic analysis, the subscript $j \in \{1, \ldots, n\}$ in the coordinates $\boldsymbol{a}_j$, $\boldsymbol{b}_j$ and $\boldsymbol{p}_j$ represents the next position of the mechanism when crank rotates the angle θ_j from its initial position ($\boldsymbol{a}_0$, $\boldsymbol{b}_0$ and $\boldsymbol{p}_0$), as shown in Fig. 3.

The following procedure is used to compute the *j-th* coordinate of the mechanism from its initial position.

First, the displacement of $\boldsymbol{a}_j$ is given in (1), where $[R_{\theta_j \boldsymbol{f}}]$ is the rotation matrix considering the vector $(\boldsymbol{f} - \mathbf{0})$ rotates an angle θ_j with respect to the initial position. This displacement can be observed in Fig. 3(a).

$$\boldsymbol{a}_j = [R_{\theta_j \boldsymbol{f}}](\boldsymbol{a}_0 - \boldsymbol{f}) + \boldsymbol{f} \tag{1}$$

The general expression of the rotation matrix with the axis-angle representation considering the rotation axis in $\hat{\boldsymbol{u}} = [\hat{u}_x, \hat{u}_y, \hat{u}_z]^T$ and the angle β, results [81], [82],

$$[R_{\beta, \hat{\boldsymbol{u}}}] = \left[I - Q_{\hat{\boldsymbol{u}}}\right] \cos(\beta) + \left[P_{\hat{\boldsymbol{u}}}\right] \sin(\beta) + Q_{\hat{\boldsymbol{u}}} \tag{2}$$

where

$$\left[Q_{\hat{\boldsymbol{u}}}\right] = \begin{bmatrix} \hat{u}_x & \hat{u}_x\hat{u}_y & \hat{u}_x\hat{u}_z \\ \hat{u}_x\hat{u}_y & \hat{u}_y & \hat{u}_y\hat{u}_z \\ \hat{u}_x\hat{u}_z & \hat{u}_y\hat{u}_z & \hat{u}_z \end{bmatrix}, \tag{3}$$

$$\left[P_{\hat{\boldsymbol{u}}}\right] = \begin{bmatrix} 0 & -\hat{u}_z & \hat{u}_y \\ \hat{u}_z & 0 & -\hat{u}_x \\ -\hat{u}_y & \hat{u}_x & 0 \end{bmatrix} \tag{4}$$

Second, the $j-th$ next position of $\boldsymbol{b}_0$ given by $\boldsymbol{b}_j$ is obtained as follows:

i) The initial vector $(\boldsymbol{b}_0 - \boldsymbol{f})$ is rotated θ_j rad around the vector $(\boldsymbol{f} - \mathbf{0})$, resulting in the point $\boldsymbol{b}'_j$. The point $\boldsymbol{b}'_j$ is obtained in (5). This relative angular displacement is shown in Fig. 3 where the lines in red color represent the mechanism in the initial position, while the lines in translucent red color indicate the mechanism with the aforementioned rotation.

$$\boldsymbol{b}'_j = [R_{\theta_j \boldsymbol{f}}](\boldsymbol{b}_0 - \boldsymbol{f}) + \boldsymbol{f} \tag{5}$$

ii) At the same time the vector $(\boldsymbol{b}'_j - \boldsymbol{a}_j)$ is rotated α_j rad around the vector $(\boldsymbol{a}_j - \mathbf{0})$ to produce the next position $\boldsymbol{b}_j$. This displacement is shown in Fig. 3(b) with its mathematical expression detailed in (6).

$$\boldsymbol{b}_j = [R_{\alpha_j, \boldsymbol{a}_j}](\boldsymbol{b}'_j - \boldsymbol{a}_j) + \boldsymbol{a}_j \tag{6}$$

In order to apply (6), it is necessary to find the angle α_j that guarantees a constant geodesic distance in r_4 of the output link through the movement in θ_j, i.e., the output link must ensure to be a rigid body. In that direction, the condition (7)

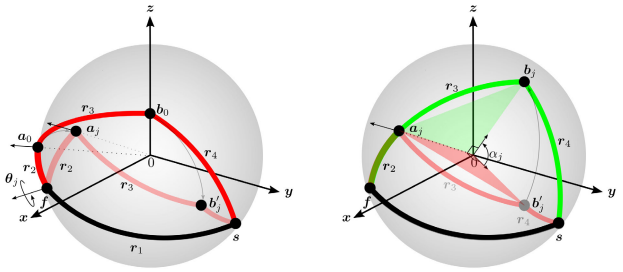

(a) Rotation of $\boldsymbol{b}_0$ around $\boldsymbol{f}$. (b) Rotation of $\boldsymbol{b}'_j$ around $\boldsymbol{a}_j$.

FIGURE 3. Sequence of the Kinematic movement of the spherical four-bar mechanism from the initial position to the $j-th$ position.

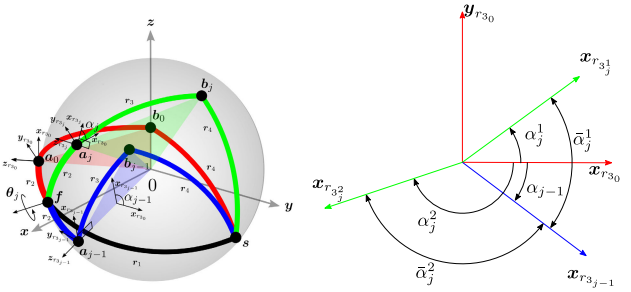

(a) Angle α_j in the coordinate system $x_{r_3} - y_{r_3} - z_{r_3}$. (b) Visualization of the angles α_j^i and α_{j-1}.

FIGURE 4. Schematic representation of the α_j movement.

must be fulfilled that relate the same distance in the vector $(\boldsymbol{b}_0 - \boldsymbol{s})$ as well as in the vector $(\boldsymbol{b}_j - \boldsymbol{s})$.

$$(\boldsymbol{b}_j - \boldsymbol{s})^T(\boldsymbol{b}_j - \boldsymbol{s}) = (\boldsymbol{b}_0 - \boldsymbol{s})^T(\boldsymbol{b}_0 - \boldsymbol{s}) \tag{7}$$

Substituting (6) in (7) results in (8).

$$\begin{aligned}(\boldsymbol{b}'_j - \boldsymbol{a}_j)^T(\boldsymbol{b}'_j - \boldsymbol{a}_j) + 2(\boldsymbol{a}_j - \boldsymbol{s})^T[R_{\alpha_j,\boldsymbol{a}_j}](\boldsymbol{b}'_j - \boldsymbol{a}_j) \\ + (\boldsymbol{a}_j - \boldsymbol{s})^T(\boldsymbol{a}_j - \boldsymbol{s}) = (\boldsymbol{b}_0 - \boldsymbol{s})^T(\boldsymbol{b}_0 - \boldsymbol{s})\end{aligned} \tag{8}$$

Rewritten (8) in terms of the angle α_j using (2) with $\hat{\boldsymbol{u}} = \boldsymbol{a}_j$ and $\beta = \alpha_j$, results in the Freudenstein's equation [83] showed in (9).

$$E\cos(\alpha_j) + F\sin(\alpha_j) + G = 0 \tag{9}$$

where:

$$\begin{aligned}E &= (\boldsymbol{a}_j - \boldsymbol{s})^T[I - Q_{\boldsymbol{a}_j}](\boldsymbol{b}'_j - \boldsymbol{a}_j), \\ F &= (\boldsymbol{a}_j - \boldsymbol{s})^T[P_{\boldsymbol{a}_j}](\boldsymbol{b}'_j - \boldsymbol{a}_j) \\ G &= (\boldsymbol{a}_j - \boldsymbol{s})^T[Q_{\boldsymbol{a}_j}](\boldsymbol{b}'_j - \boldsymbol{a}_j) - \frac{1}{2}(\boldsymbol{b}_0 - \boldsymbol{s})^T(\boldsymbol{b}_0 - \boldsymbol{s}) \\ &\quad + \frac{1}{2}(\boldsymbol{b}'_j - \boldsymbol{a}_j)^T(\boldsymbol{b}'_j - \boldsymbol{a}_j) + \frac{1}{2}(\boldsymbol{a}_j - \boldsymbol{s})^T(\boldsymbol{a}_j - \boldsymbol{s})\end{aligned} \tag{10}$$

The solution of the Freudenstein's equation (9) can produce two real solutions for the angle α_j (α_j^1 and α_j^2) when $E^2 + F^2 - G^2 \geq 0$, as is observed in (11) $\forall\, i = 1, 2$.

$$\alpha_j^i = 2atan2\left(-F + (-1)^i\sqrt{E^2 + F^2 - G^2}, (G - E)\right) \tag{11}$$

The selection of the angle α_j is determined by the angle α_j^i in (11) closer to the previous position α_{j-1} of the mechanism, i.e., the following condition is considered to set the angle α_j:

$$\alpha_j = \begin{cases}\alpha_j^1 & \textbf{If } \left|\alpha_j^1 - \alpha_{j-1}\right| < \left|\alpha_j^2 - \alpha_{j-1}\right| \\ \alpha_j^2 & \textbf{Otherwise}\end{cases} \tag{12}$$

Nevertheless, the main issue in the above condition is to find the angle α_j. In order to give a procedure to obtain the angle α_j, the following strategy is provided.

The computation of the relative angles α_j α_{j-1}, α_j^1 and α_j^2 considers the initial position of the mechanism in the points $\boldsymbol{b}_0$, $\boldsymbol{a}_0, \boldsymbol{f}$, $\boldsymbol{s}$ of Fig. 4(a) (red links). Hence, the initial angle $\alpha_0 = 0$ is set. Two different movements provided by the crank angle α_{j-1} and α_j of the spherical four-bar mechanism is shown in Fig. 4(a), both are relative to the initial configuration of the mechanism. The green plane formed by the points $\boldsymbol{b}_j$, $\boldsymbol{0}$, and $\boldsymbol{a}_j$ (plane $\boldsymbol{b}_j - \boldsymbol{0} - \boldsymbol{a}_j$) is given by the rotation of α_j rad. Meanwhile, the blue plane $\boldsymbol{b}_{j-1} - \boldsymbol{0} - \boldsymbol{a}_{j-1}$ is rotated α_{j-1} rad.

The $\psi - th$ auxiliary coordinate system $x_{r_{3_\psi}} - y_{r_{3_\psi}} - z_{r_{3_\psi}}$ is set in the point $\boldsymbol{a}_\psi$ $\forall$ $\psi \in \{0, j-1, j\}$, where the axis $z_{r_{3_\psi}}$ is collinear to the unit vector $\boldsymbol{a}_\psi - \boldsymbol{0}$, the axis $x_{r_{3_\psi}}$ is perpendicular to the axis $z_{r_{3_\psi}}$ and belong to the red plane $\boldsymbol{a}_\psi - \boldsymbol{0} - \boldsymbol{b}_\psi$ in Fig. 4(a). The $y_{r_{3_\psi}}$ is defined according to the right-hand rule.

Then, the angle α_j of the green plane $\boldsymbol{b}_j - \boldsymbol{0} - \boldsymbol{a}_j$ is obtained from α_j^i (11) closer to the previous position of the blue plane $\boldsymbol{b}_{j-1} - \boldsymbol{0} - \boldsymbol{a}_{j-1}$ which considers an angle α_{j-1}. Considering only the rotation in the axis $z_{r_{3_\psi}}$ of the coordinate system $x_{r_{3_\psi}} - y_{r_{3_\psi}} - z_{r_{3_\psi}}$ and the rotation α_j^i (11), those coordinate systems can be visualized as in Fig. 4(b), where the unit vectors of the corresponding axes are determined by $(\cos(\alpha_\psi), \sin(\alpha_\psi))$ and $(\cos(\alpha_j^i), \sin(\alpha_j^i))$. Using the al-Kashi's theorem [84] in such unit vectors, the angle $\bar{\alpha}^i$ $\forall$ $i = 1, 2$ between the vectors $(\cos(\alpha_j^i), \sin(\alpha_j^i))$ and $(\cos(\alpha_{j-1}), \sin(\alpha_{j-1}))$ are computed as follows:

$$\bar{\alpha}^i = \cos^{-1}\left(\frac{2 - \|\mathcal{V}_\alpha\|^2}{2}\right) \tag{13}$$

where

$$\mathcal{V}_\alpha = (\cos(\alpha_{j-1}) - \cos(\alpha_j^i), \sin(\alpha_{j-1}) - \sin(\alpha_j^i)) \tag{14}$$

Considering (13), the next condition is included to find the angle α_j:

$$\alpha_j = \begin{cases}\alpha_j^1 & \bar{\alpha}^1 < \bar{\alpha}^2 \\ \alpha_j^2 & \textbf{Otherwise}\end{cases} \tag{15}$$

Thus, the relative angles method focuses on determining the angle α_j to know the mechanisms' position with respect to the input relative angle θ_j.

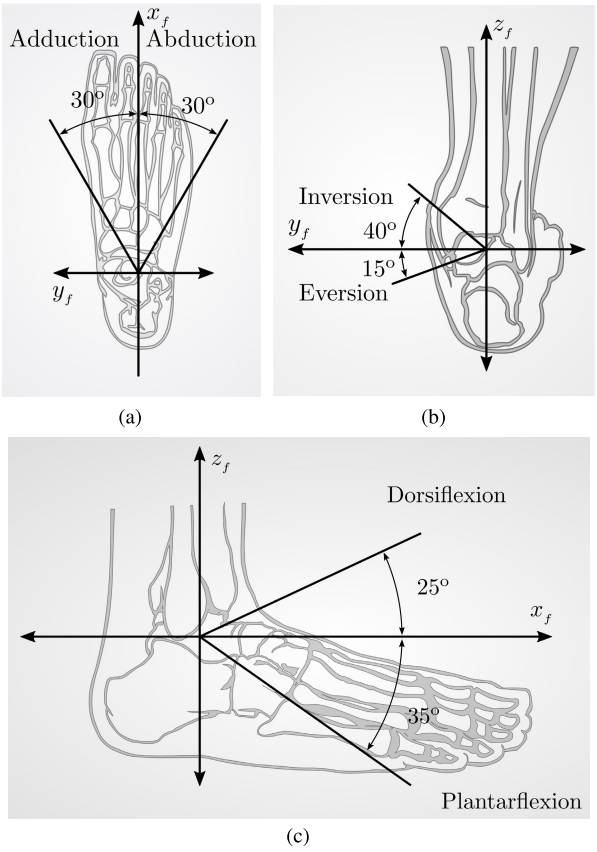

FIGURE 5. Schematic representation of the ankle movements.

Finally, the next position of the coupler point $\boldsymbol{p}_j$ due to the $j-th$ angular displacement of the crank θ_j can be obtained by using a similar procedure stated above. It is important to note that the movement equations will affect the vectors $\boldsymbol{p}_j$ and $\boldsymbol{b}_j$ in the same way because the points $\boldsymbol{p}_0$ and $\boldsymbol{b}_0$ are in the same rigid body. As a result, the position $\boldsymbol{p}_j$ is defined in (16).

$$\boldsymbol{p}_j = [R_{\alpha_j,\boldsymbol{a}_j}](\boldsymbol{p}'_j - \boldsymbol{a}_j) + \boldsymbol{a}_j \tag{16}$$

where:

$$\boldsymbol{p}'_j = [R_{\theta_j,\boldsymbol{f}}](\boldsymbol{p}_0 - \boldsymbol{f}) + \boldsymbol{f} \tag{17}$$

With (16), it is possible to obtain the path traced by the coupler point $\boldsymbol{p}_j$ for all input angles $\theta_j \in [0, 2\pi]$.

III. DIMENSIONAL SYNTHESIS OF THE SPHERICAL FOUR-BAR MECHANISM FOR THE PASSIVE ANKLE REHABILITATION

The ankle has three joints: the talocrural joint, the subtalar joint, and the inferior tibiofibular joint [85]. Those joints give rise to the movements of plantarflexion/dorsiflexion (PL/DO), adduction/abduction (AD/AB) and inversion/eversion (IN/EV) as seen in Fig. 5. Due to the above, it is possible to approximate the movement of the ankle joint to a spherical joint. The use of parallel robots have been designed for ankle rehabilitation purpose [86].

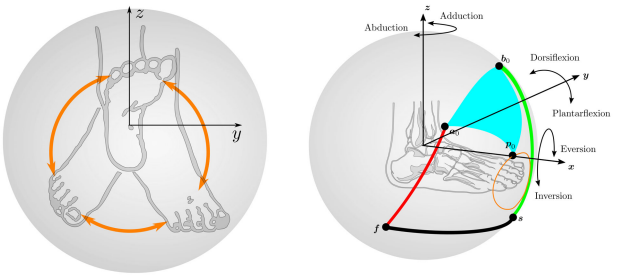

(a) Graphical representation of the ankle rehabilitation movement.

(b) Mechanism with the foot.

FIGURE 6. Sketch of the spherical mechanism for the passive ankle rehabilitation.

The considered passive rehabilitation exercise is a movement that rotates the ankle both in the y axis (PL/DO movement) and in the z axis (AD/AB movement), as shown in Fig. 6(a). The spherical 4-bar mechanism is proposed in this work to achieve such movement, as shown in Figure 6(b). It is observed that the rotation center of the mechanism coincides with the rotation center of the ankle, and the rotation axes of the foot coordinate system $x_f - y_f - z_f$ (see Fig. 5) are collinear to the rotation axes $x - y - z$ of the mechanism (see Fig. 6). Then, the tip of the foot will be guided by the mechanism's coupler point $\boldsymbol{p}_j$.

This work proposes a constrained optimization problem to carry out the dimensional synthesis of the spherical mechanism for the path generation task. In this problem, the geodesic distances of the links must be found such that the coupler point curve $\boldsymbol{p}_j$ presents the minimum error with respect to the set of points $\boldsymbol{q}_j$ describing the desired rehabilitation path, subject to the inherent constraints in the design. The formal statement of the optimization problem is presented below.

$$\min_{\boldsymbol{x}} J(\boldsymbol{x}) \tag{18}$$

Subject to:

$$g_i(\boldsymbol{x}) \leq 0, \quad \forall \quad i = 1, 2, \ldots, m \tag{19}$$

$$\boldsymbol{x}_{min} \leq \boldsymbol{x} \leq \boldsymbol{x}_{max} \tag{20}$$

In the next sections, the elements of the optimization problem are detailed.

1) OBJECTIVE FUNCTION

The main objective of the path generation task is to design a mechanism with the closest coupler point curve to the predefined set of points. In this context, the objective function (21) is related to the sum of the squared error between the $j-th$ coupler point $\boldsymbol{p}_j$ and the $j-th$ precision point $\boldsymbol{q}_j$.

$$J(\boldsymbol{x}) = \sum_{j=1}^{n} \left[(\boldsymbol{q}_j - \boldsymbol{p}_j)^T (\boldsymbol{q}_j - \boldsymbol{p}_j) \right] \tag{21}$$

The desired path for the ankle rehabilitation routine is shown in Fig. 7, where twenty-one precision points (marked

TABLE 2. Desired points describing the ankle rehabilitation trajectory.

	$\boldsymbol{q}_j = [q_{x_j}, q_{y_j}, q_{z_j}]^T$		
j	q_{x_j}	q_{y_j}	q_{z_j}
1	0.9063	-0.2423	0.3461
2	0.9059	-0.1114	0.4083
3	0.9048	0.0470	0.4231
4	0.9032	0.2078	0.3754
5	0.9027	0.3382	0.2658
6	0.9054	0.4093	0.1122
7	0.9123	0.4056	-0.0550
8	0.9219	0.3302	-0.2023
9	0.9311	0.2031	-0.3027
10	0.9374	0.0541	-0.3437
11	0.9396	-0.0885	-0.3303
12	0.9374	-0.2069	-0.2797
13	0.9311	-0.2961	-0.2126
14	0.9219	-0.3588	-0.1457
15	0.9123	-0.4000	-0.0870
16	0.9054	-0.4230	-0.0344
17	0.9027	-0.4297	0.0204
18	0.9032	-0.4203	0.0866
19	0.9048	-0.3912	0.1677
20	0.9059	-0.3348	0.2589
21	0.9063	-0.2423	0.3461

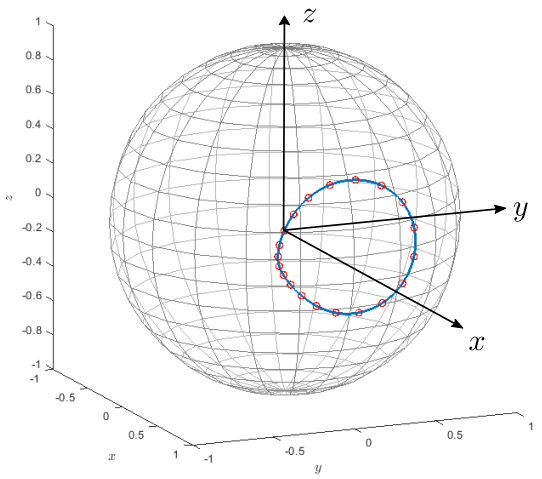

FIGURE 7. Schematic representation of the desired path for ankle rehabilitation.

in small red circles) are selected ($n = 21$). The numeric values of those desired points are presented in Table 2.

One crucial issue is guaranteeing that the ankle rotation angles stay within their anatomical limits when the mechanism moves through the precision points. Table 3 presents the maximum limits of ankle movement.

The angular displacements ω_y and ω_z related to the PL/DO movement and the AD/AB ankle movements, respectively, are computed using the proposed rehabilitation routine given in Table 2. For this purpose, a unit vector $\boldsymbol{h}$ is defined pointing to the rehabilitation trajectory, as shown in Figure 8. It is

TABLE 3. Maximum movement allowed at the ankle [87].

Movement axis	Ankle movement	Maximum motion range
$\curvearrowleft z_f$	Adduction (AD)	$25° - 30°$
$\curvearrowright z_f$	Abduction (AB)	$25° - 30°$
$\curvearrowleft y_f$	Plantarflexion (PL)	$25° - 35°$
$\curvearrowright y_f$	Dorsiflexion (DO)	$20° - 25°$
$\curvearrowleft x_f$	Inversion (IN)	$35° - 40°$
$\curvearrowright x_f$	Eversion (EV)	$15°$

assumed that the vector $\boldsymbol{h}$ presents two sequential rotations. The first rotation (ω_z) is with respect to the z axis, and the latter (ω_y) is with respect to the y axis. The j-th value of the angle ω_{y_j} and ω_{z_j} at any position of the desired trajectory can be determined by using (22) and (23), respectively.

$$\omega_{y_j} = -\sin^{-1}\left(q_{z_j}\right) \tag{22}$$

$$\omega_{z_j} = \text{atan2}\left(q_{y_j}, q_{x_j}\right) \tag{23}$$

Fig. 8(b) shows the angular position of both ω_y and ω_z during a complete cycle of the rehabilitation trajectory. As observed, the values of the angles ω_y and ω_z remain within the maximum allowed limits presented in Table 3 for the PL/DO and AD/AB movements. These limits are marked with dotted lines. Then, the proposed path for the ankle rehabilitation routine is validated.

2) DESIGN VARIABLES

The design variables are the kinematic parameters of the spherical mechanism. In this case, these variables are related to the coordinates of vectors $\boldsymbol{f}, \boldsymbol{a}_0, \boldsymbol{s}, \boldsymbol{b}_0$ and $\boldsymbol{p}_0$ in the mechanism initial position. However, since these vectors must lie on the surface of a unit sphere, then these must be represented as unit vectors (normalized vector). Let the corresponding units vectors have the same directions that the non-zero vectors $\bar{\boldsymbol{f}} = [\bar{f}_x, \bar{f}_y, \bar{f}_z]^T$, $\bar{\boldsymbol{a}}_0 = [\bar{a}_{0x}, \bar{a}_{0y}, \bar{a}_{0z}]^T$, $\bar{\boldsymbol{s}} = [\bar{s}_x, \bar{s}_y, \bar{s}_z]^T$, $\bar{\boldsymbol{b}}_0 = [\bar{b}_{0x}, \bar{b}_{0y}, \bar{b}_{0z}]^T$ and $\bar{\boldsymbol{p}}_0 = [\bar{p}_{0x}, \bar{p}_{0y}, \bar{p}_{0z}]^T$, the units vectors $\boldsymbol{f}, \boldsymbol{a}_0, \boldsymbol{s}, \boldsymbol{b}_0$ and $\boldsymbol{p}_0$ can be computed as in (25)-(28).

$$\boldsymbol{a}_0 = \bar{\boldsymbol{a}}_0 / \parallel \bar{\boldsymbol{a}}_0 \parallel \tag{24}$$

$$\boldsymbol{b}_0 = \bar{\boldsymbol{b}}_0 / \parallel \bar{\boldsymbol{b}}_0 \parallel \tag{25}$$

$$\boldsymbol{f} = \bar{\boldsymbol{f}} / \parallel \bar{\boldsymbol{f}} \parallel \tag{26}$$

$$\boldsymbol{s} = \bar{\boldsymbol{s}} / \parallel \bar{\boldsymbol{s}} \parallel \tag{27}$$

$$\boldsymbol{p}_0 = \bar{\boldsymbol{p}}_0 / \parallel \bar{\boldsymbol{p}}_0 \parallel \tag{28}$$

In this case, the design variable vector includes the elements (coordinates) of the non-zero vectors $\bar{\boldsymbol{f}}$, $\bar{\boldsymbol{a}}_0$, $\bar{\boldsymbol{s}}$, $\bar{\boldsymbol{b}}_0$ and $\bar{\boldsymbol{p}}_0$.

On the other hand, the proposed dimensional synthesis in the path generation for ankle rehabilitation is without prescribed timing since it is not required to guarantee that a specific value in the crank movement produces a particular movement of the coupler point. Hence, the n angular displacements of the crank $\theta_j \in \{\theta_1, \theta_2, \ldots, \theta_n\}$ that produce the n

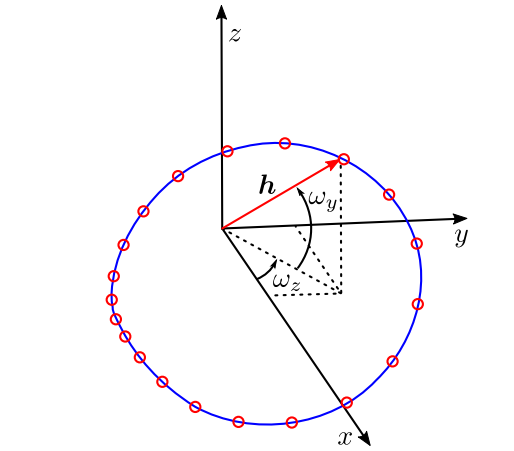

(a) Desired path in the Cartesian space.

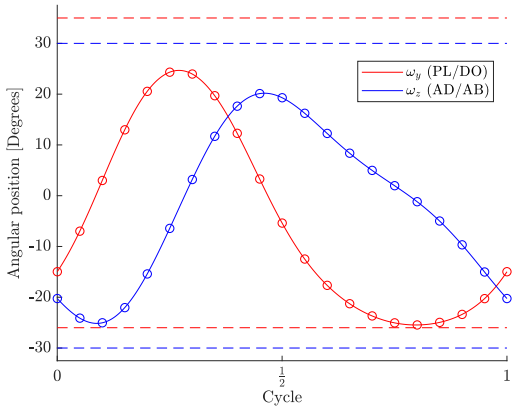

(b) Desired path in the angular space.

FIGURE 8. Desired path for the rehabilitation routine in the Cartesian and angular space.

coordinates of the coupler point are included in the design variable vector.

Finally, the design variable vector $\boldsymbol{x} \in \boldsymbol{R}^{15+n}$ is presented in (29).

$$\boldsymbol{x} = \left[\bar{a}_{0x}, \bar{a}_{0y}, \bar{a}_{0z}, \bar{b}_{0x}, \bar{b}_{0y}, \bar{b}_{0z}, \bar{f}_x, \bar{f}_y, \bar{f}_z, \bar{s}_x, \bar{s}_y, \bar{s}_z, \bar{p}_{0x}, \bar{p}_{0y}, \bar{p}_{0z}, \theta_1, \theta_2, \ldots, \theta_n\right] \tag{29}$$

3) CONSTRAINTS

One important constraint is to fulfill the existence of an assembled mechanism through its movements, i.e., the solution of the mechanism kinematics (11) must be real numbers. Therefore, a hard constraint [22] is included to satisfy that condition. This constraint is given in (30).

$$g_1(\boldsymbol{x}) : -(E^2 + F^2 - G^2) \leq 0 \tag{30}$$

The evaluation of the hard constraint at a possible problem solution must be done before the computation of the objective function and the remaining constraints. In the case that the hard constraint is not satisfied, the objective function will take a high value, and the remaining constraints will be evaluated, as observed in Algorithms 1 and 2 of Section IV.

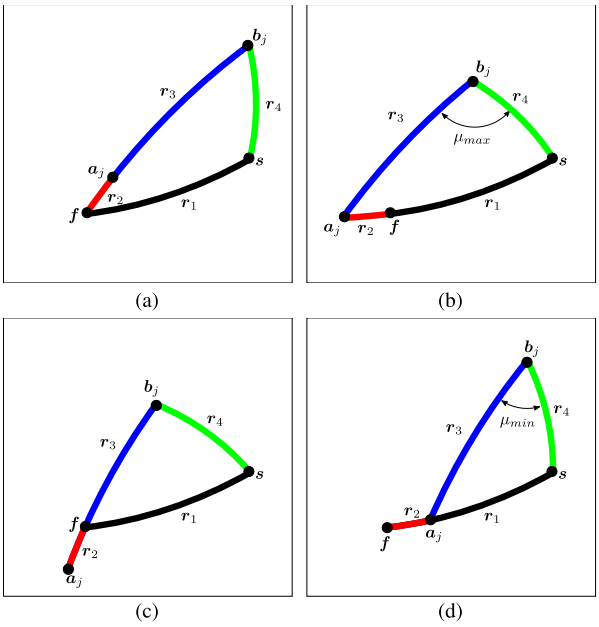

FIGURE 9. Critical positions of the spherical crank-rocker mechanism.

Other constraint involves that the mechanism presents the crank-rocker configuration [80], which is achieved as long as the four critical positions of the crank r_2 (see Fig. 9) meet the criteria in (31)-(37).

$$r_2 + r_3 \leq r_1 + r_4 \tag{31}$$
$$r_2 + r_1 \leq r_3 + r_4 \tag{32}$$
$$r_3 - r_2 \geq r_1 - r_4 \tag{33}$$
$$r_3 - r_2 \geq r_4 - r_1 \tag{34}$$
$$r_1 - r_2 \geq r_3 - r_4 \tag{35}$$
$$r_1 - r_2 \geq r_4 - r_3 \tag{36}$$
$$r_2 - r_4 \leq r_3 + r_1 \tag{37}$$

It is observed when the crank r_2 is aligned with r_3, as shown in Fig. 9(a), it is necessary to fulfill the inequality (31). When r_2 is aligned with r_1 (see Fig. 9(b)), the condition (32) must fulfill. In the case where r_2 is over r_3, as shown in Fig. 9(b), there are two conditions; the first one must satisfy (33) whether $r_1 < r_4$, and the second one implies that $r_4 < r_1$ and the inequality (34) must satisfy. In the last case where r_2 is over r_1, shown in Fig. 9(d), the inequality (35) must fulfill when $r_3 > r_4$, otherwise the inequality (36) must satisfy when $r_4 > r_3$.

According to the Grashof criterion [88], the resulting independent constraints of (31)-(37) for the optimization problem that guarantee a crank-rocker configuration in the mechanism

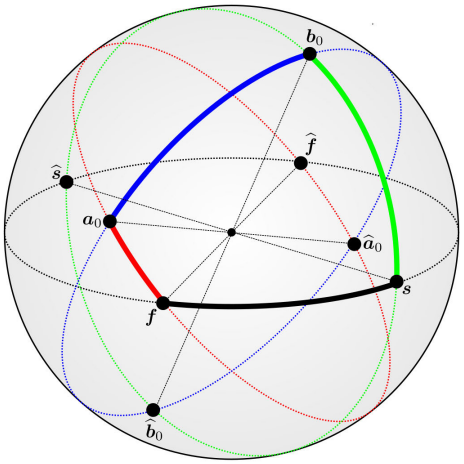

FIGURE 10. Representation of the base and supplementary configurations in the spherical four-bar mechanism.

TABLE 4. Supplementary configurations for the spherical four-bar mechanism.

Spherical Mechanism	
Original	Reflection
$\boldsymbol{f}, \boldsymbol{a}_0, \boldsymbol{b}_0, \boldsymbol{s}$	$\widehat{\boldsymbol{f}}, \widehat{\boldsymbol{a}}_0, \widehat{\boldsymbol{b}}_0, \widehat{\boldsymbol{s}}$
$\widehat{\boldsymbol{f}}, \boldsymbol{a}_0, \boldsymbol{b}_0, \boldsymbol{s}$	$\boldsymbol{f}, \widehat{\boldsymbol{a}}_0, \widehat{\boldsymbol{b}}_0, \widehat{\boldsymbol{s}}$
$\boldsymbol{f}, \widehat{\boldsymbol{a}}_0, \boldsymbol{b}_0, \boldsymbol{s}$	$\widehat{\boldsymbol{f}}, \boldsymbol{a}_0, \widehat{\boldsymbol{b}}_0, \widehat{\boldsymbol{s}}$
$\boldsymbol{f}, \boldsymbol{a}_0, \widehat{\boldsymbol{b}}_0, \boldsymbol{s}$	$\widehat{\boldsymbol{f}}, \widehat{\boldsymbol{a}}_0, \boldsymbol{b}_0, \widehat{\boldsymbol{s}}$
$\boldsymbol{f}, \boldsymbol{a}_0, \boldsymbol{b}_0, \widehat{\boldsymbol{s}}$	$\widehat{\boldsymbol{f}}, \widehat{\boldsymbol{a}}_0, \widehat{\boldsymbol{b}}_0, \boldsymbol{s}$
$\widehat{\boldsymbol{f}}, \widehat{\boldsymbol{a}}_0, \boldsymbol{b}_0, \boldsymbol{s}$	$\boldsymbol{f}, \boldsymbol{a}_0, \widehat{\boldsymbol{b}}_0, \widehat{\boldsymbol{s}}$
$\boldsymbol{f}, \widehat{\boldsymbol{a}}_0, \widehat{\boldsymbol{b}}_0, \boldsymbol{s}$	$\widehat{\boldsymbol{f}}, \boldsymbol{a}_0, \boldsymbol{b}_0, \widehat{\boldsymbol{s}}$
$\boldsymbol{f}, \boldsymbol{a}_0, \widehat{\boldsymbol{b}}_0, \widehat{\boldsymbol{s}}$	$\widehat{\boldsymbol{f}}, \widehat{\boldsymbol{a}}_0, \boldsymbol{b}_0, \boldsymbol{s}$

are stated in (38)-(40).

$$g_2(\boldsymbol{x}): \; r_2 + r_1 - r_3 - r_4 \leq 0 \tag{38}$$
$$g_3(\boldsymbol{x}): \; r_2 + r_3 - r_1 - r_4 \leq 0 \tag{39}$$
$$g_4(\boldsymbol{x}): \; r_2 + r_4 - r_1 - r_3 \leq 0 \tag{40}$$

On the other hand, the spherical mechanism has different supplementary configurations. For instance, in the base configuration of the spherical mechanism shown in Fig. 10, and composed by the points $\boldsymbol{f}, \boldsymbol{a}_0, \boldsymbol{b}_0, \boldsymbol{s}$, where it is observed that such configuration given by the links in continuous color lines consider the least geodesic distance between these points. Nevertheless, the other fifteen supplementary configurations can be set in the links for the spherical mechanism, which are kinematically equivalent. Those configurations are formed by using supplementary points $\widehat{\boldsymbol{f}}, \widehat{\boldsymbol{a}}_0, \widehat{\boldsymbol{s}}$ and $\widehat{\boldsymbol{b}}_0$ given by the intersections of each pair of dotted rings displayed Fig. 10. All supplementary configurations of the spherical mechanism are presented in Table 4.

From sixteen configurations, eight of them are reflections of others. Therefore, the seven configurations of the mechanism can be stated by replacing two or four links of the base mechanism (formed by the points $\boldsymbol{f}$, $\boldsymbol{a}_0$, $\boldsymbol{b}_0$, $\boldsymbol{s}$) with their respective supplementary geodesic distance (according to the supplementary points).

It is essential to establish a criterion that allows selecting the configuration with the least geodesic distance between these points. For that purpose, the sum of the geodesic distances of two links must be less than π rad [80]. That condition is included as constraints and they are presented in (41)-(46).

$$g_5(\boldsymbol{x}): \; r_2 + r_3 - \pi \leq 0 \tag{41}$$
$$g_6(\boldsymbol{x}): \; r_2 + r_4 - \pi \leq 0 \tag{42}$$
$$g_7(\boldsymbol{x}): \; r_2 + r_1 - \pi \leq 0 \tag{43}$$
$$g_8(\boldsymbol{x}): \; r_3 + r_4 - \pi \leq 0 \tag{44}$$
$$g_9(\boldsymbol{x}): \; r_3 + r_1 - \pi \leq 0 \tag{45}$$
$$g_{10}(\boldsymbol{x}): \; r_4 + r_1 - \pi \leq 0 \tag{46}$$

The force transmitted from the crank link to the output link is another criterion to be considered in the spherical mechanism for ankle rehabilitation. This criterion is related to the transmission angle μ shown in Fig. 2. The suitable interval given in [89] ($\mu \in [\frac{\pi}{4}, \frac{3\pi}{4}]$ rad) is used in this paper. Then, the constraints in (47)-(48) is included for guaranteeing a suitable force transmission.

$$g_{11}(\boldsymbol{x}): \frac{\pi}{4} - \mu_{min} \leq 0 \tag{47}$$
$$g_{12}(\boldsymbol{x}): \mu_{max} - \frac{3\pi}{4} \leq 0 \tag{48}$$

where

$$\mu_{min} = \left\| \cos^{-1}\left(\frac{\cos(r_1 - r_2) - \cos(r_4)\cos(r_3)}{\sin(r_4)\sin(r_3)} \right) \right\| \tag{49}$$
$$\mu_{max} = \left\| \cos^{-1}\left(\frac{\cos(r_1 + r_2) - \cos(r_4)\cos(r_3)}{\sin(r_4)\sin(r_3)} \right) \right\| \tag{50}$$

The limits of the transmission angle μ are obtained by using the cosines law for spherical triangles [90]. Applying this formalism requires that the formed triangle remains in a unit sphere with geodesic distances of its sides less than π rad. This requirement is satisfied whether (41)-(46) are accomplished.

The minimum transmission angle μ_{min} is obtained when the crank r_2 is on the ground link r_1, as shown in Fig. 9(d). The formed triangle is given by $r_1 - r_2$, r_3 and r_4. The maximum transmission angle μ_{max} is obtained when the input handle r_2 is aligned with r_1, as shown in Fig. 9(b). The formed triangle is given by $r_1 + r_2$, r_3 and r_4.

Another condition in the spherical mechanism synthesis is related to the movement of angles θ_j. The constraint (51) assures the counterclockwise rotation of the crank.

$$g_{12+i}(\boldsymbol{x}): \quad \theta_i - \theta_{i+1} \leq 0, \; \forall \, i = 1, 2, \ldots, n-1 \tag{51}$$

Finally, the last constraint given in (20) involves the allowed bounds in the design variable $\boldsymbol{x}$. The minimum $\boldsymbol{x}_{min} \in R^{15+n}$ and maximum $\boldsymbol{x}_{max} \in R^{15+n}$ bounds are presented

in (52)-(53), respectively.

$$\boldsymbol{x}_{min} = [-1,-1,-1,-1,-1,-1,-1,-1,-1,\\ -1,-1,-1,-1,-1,-1,0,\ldots,0] \quad (52)$$

$$\boldsymbol{x}_{max} = [\ 1,\ 1,\ 1,\ 1,\ 1,\ 1,\ 1,\ 1,\ 1,\\ 1,\ 1,\ 1,\ 1,\ 1,\ 1,2\pi,\ldots,2\pi] \quad (53)$$

IV. DIFFERENTIAL EVOLUTION

The dimensional synthesis problem stated in Section III is solved by using two different evolutionary algorithms. The differential evolution variants $DE/rand/1/bin$ and $DE/best/1/bin$ are implemented because they present a good approximation to a good solution in a reasonable time [91], and they have recently shown outstanding results compared with the state-of-the-art algorithms solving mechanism synthesis problems [23] as is observed in circle chart in Fig. 1.

The theory of evolution of species dictates that individuals of a species mutate and interbreed over generations, allowing the genes of the best individuals of the species to be passed on to the next generation. Thus, changes in the species will enable adaptations that improve individuals to preserve it.

The Differential Evolution (DE) algorithm is a stochastic search method [34] inspired by the theory of evolution of species belonging to the classification of evolutionary algorithms. The possible solutions (design variable vector) in the optimization problem are the individuals of a population. Thus, those solutions evolve to increase the fitness of the population (the minimization of the objective function) and hence, to find the aptest solution to the problem.

The pseudo-code of the DE algorithm is presented in the Algorithm 1. It starts with a population of Np randomly generated individuals within the limits of the search space of design variables. Once the initial population is established, subsequent generations of individual populations are created up to a maximum generation G_{max}. The current population in a particular generation $\mathbf{x}^{i,G}\ \forall\ i = 1,\ldots,Np$ is mutated and crossed to generate the child population $\mathbf{u}^{i,G}\ \forall\ i = 1,\ldots,Np$. In the case of the DE variant $DE/rand/1/bin$, it performs a random mutation of the population's individuals with one difference vector and also considers a binomial crossover. In the case of $DE/best/1/bin$, it performs an elitist mutation based on the knowledge of the best population's individual with one difference vector and considers a binomial crossover. The mutation and crossover of the $j-th$ element for the $i-th$ individual in the generation G are displayed in (54), as shown at the bottom of the page, where $F \in [F_{min}, F_{max}]$ is known as the scale factor and is randomly generated at each generation between its minimum F_{min} and maximum F_{max} values, and $CR \in [0,1]$ is a constant value that set the probability factor to pass genes of the parent vector or the mutant vector. The superscript $\bar{r}_x$ of vectors are related to the $\bar{r}_x - th$ individual randomly taken from the current population and different from the $i - th$ parent individual, i.e., $\bar{r}_1 \neq \bar{r}_2 \neq \bar{r}_3 \neq i$, while the superscript $best$ is related to the best individual in the population (the individual with the lowest performance function value).

Once the child population is created, it competes with the parent population. The individual (solution) with the best fitness pass to the next generation $G+1$.

Due to the nature of the original DE algorithm that is used to solve unconstrained optimization problems, in some works, the constrained optimization problems are transformed into unconstrained ones through diverse indirect methods [92], [93]. In this work and according to the taxonomy in [94], the method of separation of objective function and constraints proposed by Deb [95] is considered, where the optimization problem is not transformed. This method keeps the objective function and constraint violation separate in the algorithm selection process. One of the most well-liked and efficient methods for handling constraints is Deb's method, which uses the criteria listed below as a constraint handler to determine which of two individuals best fits the problem (the fittest solution).

1) Any feasible solution is preferred to an infeasible one.
2) Between two feasible solutions, the one with the better objective function is preferred.
3) Between two infeasible solutions, the one with the smallest distance of violated constraints is preferred.

Mutation and crossover of DE/rand/1/bin:

$$\mathbf{u}^{i,j,G} = \begin{cases} \overbrace{\overbrace{\mathbf{v}^{i,j,G} = \mathbf{x}^{\bar{r}_1,j,G} + F(\mathbf{x}^{\bar{r}_2,j,G} - \mathbf{x}^{\bar{r}_3,j,G})}^{Mutation} \ \textbf{if}\ (rand(0,1) < CR)\ \textbf{or}\ j == j_{rad}}^{Crossover} \\ \mathbf{v}^{i,j,G} = \mathbf{x}^{i,j,G} \qquad \textbf{otherwise} \end{cases} \quad (54)$$

Mutation and crossover of DE/best/1/bin:

$$\mathbf{u}^{i,j,G} = \overbrace{\begin{cases} \overbrace{\mathbf{v}^{i,j,G} = \mathbf{x}^{best,j,G} + F(\mathbf{x}^{\bar{r}_1,j,G} - \mathbf{x}^{\bar{r}_2,j,G})}^{Mutation} \ \textbf{if}\ (rand(0,1) < CR)\ \textbf{or}\ j == j_{rad} \\ \mathbf{v}^{i,j,G} = \mathbf{x}^{i,j,G} \qquad \textbf{otherwise} \end{cases}}^{Crossover}$$

Algorithm 1 Differential Evolution Algorithm

Begin
  $G \leftarrow 1$
  Create the random initial population $\mathbf{x}^{i,G}$ $\forall_i = 1, \ldots, Np$.
  Evaluate $J(\mathbf{x}^{i,G})$ $\forall i = 1, \ldots, Np$ (Algorithm 2).
  Evaluate $\phi(\mathbf{x}^{i,G})$ $\forall_i = 1, \ldots, Np$ (55)
  while $G \leq G_{max}$ **do**
    for $i \leftarrow 1$**to**N_p **do**
      Create the mutant vector $\mathbf{v}^{i,G}$ using the differential mutation in (54).
      Create the child individual $\mathbf{u}^{i,G}$ with the binominal crossover in (54).
      Evaluate the objective function $J(\mathbf{u}^{i,G})$ (Algorithm 2).
      Evaluate the constraints $\phi(\mathbf{u}^{i,G})$ (55).
      Select the individual between $\mathbf{x}^{i,G}$ and $\mathbf{u}^{i,G}$ using the Deb's criterion.
    end for
    $G \leftarrow G + 1$
  end while
End

At the end of the optimization process, the population in the last generation will contain the best individuals (solutions), and the best of them is selected as the optimal design variable vector of the problem.

On the other hand, in Deb's criterion is observed that the computation of the objective function and the constraint distance (distance of violated constraints) is required. The details of the objective function evaluation of the dimensional synthesis of the spherical four-bar mechanism for ankle rehabilitation are displayed in Algorithm 2, and the constraint distance computation is shown in (55).

$$\phi = \sum_{i=1}^{n+11} max\,(0, g_i\,(\boldsymbol{x})) \tag{55}$$

V. RESULTS

The results obtained by solving the synthesis problem of the spherical mechanism for path generation in passive ankle rehabilitation are presented in this Section. First, the performance of DE algorithms is presented through the analysis of descriptive statistics with the aim of finding the individual (mechanism design solution) with the smallest position error between the precision points and the coupler point of the mechanism. Subsequently, the mechanism's simulation results are analyzed to validate the mechanism's performance when performing the proposed rehabilitation routine. Finally, the physical prototype of the ankle rehabilitation mechanism manufactured with a 3D printer is presented.

A. PERFORMANCE ANALYSIS OF THE OPTIMIZERS

This section presents the results of the obtained solutions in the DE variants $DE/rand/1/bin$ and $DE/best/1/bin$ through thirty executions of the algorithms.

Algorithm 2 Evaluation of the Performance Function for the Particular Optimization Problem

Input: $x = \left[\bar{a}_{0x}, \bar{a}_{0y}, \bar{a}_{0z}, \bar{b}_{0x}, \bar{b}_{0y}, \bar{b}_{0z}, \bar{f}_x, \bar{f}_y, \bar{f}_z, \bar{s}_x, \bar{s}_y, \bar{s}_z, \bar{p}_{0x}, \bar{p}_{0y}, \bar{p}_{0z}, \theta_1, \theta_2, \ldots, \theta_n\right]$
Output: J

Begin
  $\boldsymbol{a}_0 = \bar{\boldsymbol{a}}_0 / \parallel \bar{\boldsymbol{a}}_0 \parallel$
  $\boldsymbol{b}_0 = \bar{\boldsymbol{b}}_0 / \parallel \bar{\boldsymbol{b}}_0 \parallel$
  $\boldsymbol{f} = \bar{\boldsymbol{f}} / \parallel \bar{\boldsymbol{f}} \parallel$
  $\boldsymbol{s} = \bar{\boldsymbol{s}} / \parallel \bar{\boldsymbol{s}} \parallel$
  $\boldsymbol{p}_0 = \bar{\boldsymbol{p}}_0 / \parallel \bar{\boldsymbol{p}}_0 \parallel$
  Compute r_1, r_2, r_3, r_4
  $\alpha_0 \leftarrow 0$
  $J \leftarrow 0$
  for $j \leftarrow 1$ **to** n **do**
    Compute $\boldsymbol{a}_j$ (1)
    Compute $\boldsymbol{b}_j$ (6)
    Compute E, F, G (10)
    if $(E^2 + F^2 - G^2) < 0$ **then**
      $J \leftarrow 10000$
      Break
    end if
    Compute α_j^i (15)
    Compute $\boldsymbol{p}_j$ (16)
  end for
  Calcular J (21)
End

A PC with an Intel Core(TM) i5 processor at 1.6GHz and 12GB of RAM is used to solve with the DE variants ($DE/rand/1/bin$ and $DE/best/1/bin$), the mechanism synthesis problem for passive ankle rehabilitation. In order to find good solutions and provide a representative and meaningful comparative analysis, the configuration parameters of DE variants are tuned by a hand procedure [96]. This procedure consists of systematically varying the crossover factor $CR \in [0, 1]$ with increments of 0.05 units in its permitted interval. The minimum and maximum values for the scale factor F are set as $F_{min} = 0.3$ and $F_{max} = 0.9$. A population number of $Np = 100$ individuals with $G_{max} = 7000$ generations is also chosen, i.e., the maximum number of objective function evaluation is 700000, in both algorithms.

Thirty executions are performed at each value of CR with the previously mentioned algorithm parameter settings. At each execution, the objective function value of the best solution is stored, and a data set (sample) consists of the thirty best solutions obtained from the thirty algorithm executions with a specific CR value.

The summary of the characteristics of samples obtained by DE variants per each CR value is shown in Table 5. The first column of such a table represents the DE variant. The second column displays the chosen CR values. The third column to

TABLE 5. Descriptive statistics of the results obtained through thirty executions of DE variants with different values of *CR*.

Algorithm	CR	Mean(J)	σ(J)	Minimum(J)	Maximum(J)	ϕ	IS
DE/rand/1/bin	0.05	1.2294	5.4564e-01	5.1548e-1	2.4912	0	0
DE/rand/1/bin	0.10	2.4095e1	2.3493e1	2.4239	7.2761e1	0	7
DE/rand/1/bin	0.15	4.5638e1	2.0134e1	2.6913e1	6.9437e1	2.0577e-4	30
DE/rand/1/bin	0.20	4.2378e1	2.1647e1	6.9321	1.9701e1	1.5968e-3	30
DE/rand/1/bin	0.25	3.0981e6	1.2560e7	2.1812e1	6.2964e7	1.1595e-2	30
DE/rand/1/bin	0.30	4.7294e1	2.0908e1	1.9450e1	6.5653e1	4.3218e-2	30
DE/rand/1/bin	0.35	1.9989e6	1.0948e7	7.2698e1	4.7948e1	3.4355e-2	30
DE/rand/1/bin	0.40	9.9972e4	5.4735e5	6.3821e1	1.2803e1	2.3215e-2	30
DE/rand/1/bin	0.45	2.2986e6	1.0555e7	6.4441e1	4.5055e1	1.0345e-4	30
DE/rand/1/bin	0.50	4.6300e1	2.3125e1	1.5965	7.7843e1	0	28
DE/rand/1/bin	0.55	4.2293e1	2.3345e1	3.4009	5.9662e1	0	26
DE/rand/1/bin	0.60	3.2652e1	2.4223e1	1.8537	7.4886e1	0	18
DE/rand/1/bin	0.65	1.0829e1	1.9301e1	9.9992e-1	3.0481e1	0	6
DE/rand/1/bin	0.70	1.2789	7.4006e-1	3.6336e-1	3.2708	0	0
DE/rand/1/bin	0.75	4.2961e-1	4.5868e-1	1.4966e-2	1.4724	0	0
DE/rand/1/bin	0.80	8.8656e-2	3.3640e-1	4.2659e-4	1.8478	0	0
DE/rand/1/bin	0.85	4.7939e-2	2.0630e-1	3.7743e-4	1.1370	0	0
DE/rand/1/bin	0.90	8.8208e-3	1.7176e-2	1.2028e-4	4.4998e-2	0	0
DE/rand/1/bin	**0.95**	**7.2224e-3**	**1.5865e-2**	**1.1929e-4**	**4.4957e-2**	**0**	**0**
DE/rand/1/bin	1.00	4.0065e1	2.6515e1	3.0316	7.2367	0	20
DE/best/1/bin	0.05	9.6748e-2	2.6819e-1	6.2300e-3	1.5087	0	0
DE/best/1/bin	0.10	3.9437e-1	7.6172e-1	1.4612e-2	3.0067	0	0
DE/best/1/bin	0.15	2.3822e-1	3.3415e-1	1.5979e-2	1.3963	0	0
DE/best/1/bin	0.20	4.1700e-1	5.0065e-1	1.8262e-2	1.9853	0	0
DE/best/1/bin	0.25	4.7553e-1	6.4676e-1	9.2657e-3	2.4328	0	0
DE/best/1/bin	0.30	3.2917e-1	5.6454e-1	2.0286e-3	2.5932	0	0
DE/best/1/bin	0.35	3.5281e-1	5.4829e-1	1.2935e-3	2.0460	0	0
DE/best/1/bin	0.40	3.9143e-1	6.7027e-1	6.0685e-4	2.2756	0	0
DE/best/1/bin	0.45	3.7057e-1	5.5009e-1	6.8804e-4	1.8640	0	0
DE/best/1/bin	0.50	4.1100e-1	7.2235e-1	3.5156e-4	2.4072	0	0
DE/best/1/bin	0.55	5.6448e-1	7.7227e-1	1.6215e-4	2.2218	0	0
DE/best/1/bin	0.60	3.7013e-1	6.5183e-1	3.3557e-4	2.1190	0	0
DE/best/1/bin	0.65	5.3726e-1	7.0251e-1	1.5453e-4	1.8712	0	0
DE/best/1/bin	0.70	3.5568e-1	6.7703e-1	1.5269e-4	2.2652	0	0
DE/best/1/bin	0.75	2.1248e-1	5.0633e-1	1.2702e-4	1.7717	0	0
DE/best/1/bin	**0.80**	**5.8958**	**1.6301e1**	**1.2034e-4**	**3.3380e1**	**0**	**4**
DE/best/1/bin	0.85	1.0581e1	2.0929e1	2.2617e-4	5.9378e1	0	10
DE/best/1/bin	0.90	2.3136e1	2.4863e1	1.5375e-2	3.3459	0	18
DE/best/1/bin	0.95	4.4974e6	1.4830e7	9.6582e-2	6.7560	0	24
DE/best/1/bin	1.00	2.9980e6	7.4274e6	1.3914e1	2.6983e7	1.9483e-2	30

the sixth column presents the average, standard deviation, and the solution with the minimum and maximum performance function value obtained through the thirty executions (sample), respectively. Finally, the seventh column contains the constraint distance of the solution with the minimum objective function value, and the eighth column shows the number of Infeasible Solutions (IS), i.e., the number of solutions in the sample that did not find at least one feasible solution through the optimization process.

Through the results of the descriptive statistics shown in Table 5, the following is observed:

- The best objective function values is when the crossover value is set as $CR = 0.95$ and $CR = 0.8$ for the $DE/rand/1/bin$ ($J = 1.1929e-4$) and $DE/best/1/bin$ ($J = 1.2034e-4$), respectively (see fifth column). The small percentage difference between both objective function values is 0.87%. Nevertheless, for these same DE variants and *CR* values, the individual with the maximum performance (the worst solution) in $DE/best/1/bin$ presents an increment of 57.14% from the worst solution in $DE/rand/1/bin$ (see the sixth column). On the other hand, observing the standard

deviation (fourth column), a small value of the standard deviation indicates the convergence of the thirty executions toward a small region of the search space. In this case the $DE/rand/1/bin$ with $CR = 0.95$ presents the smaller value. This indicates that the $DE/rand/1/bin$ algorithm using the value of $CR = 0.95$ is more reliable, and also it provides the best solution to the synthesis problem of the spherical mechanism for path generation in ankle rehabilitation.

- When the $DE/best/1/bin$ considers the crossover value interval in $CR \in [0.4, 0.85]$, it finds solutions near the best ones (see fifth column). Nevertheless, through the thirty executions, the $DE/best/1/bin$ does not converge towards the best solution since the sample's mean has a higher value than the corresponding best individual (see third and fifth column). The behavior of the $DE/best/1/bin$ is attributed to the premature convergence to local solutions due to the incorporation of the best individual in the mutation process, which makes the exploitation of solutions more exhaustive (54). In contrast, the $DE/rand/1/bin$ algorithm found promising results in a smaller crossover value interval than the corresponding in $DE/best/1/bin$. The interval in the crossover value is $CR \in [0.8, 0.95]$ (see fifth column). The main difference is the mean of the sample (see the third column) in that interval presents a smaller value than the one obtained in the $DE/best/1/bin$. This implies less diversity of solutions among different executions of the $DE/rand/1/bin$. This behavior is attributed to the pseudo-random selection of individuals in the mutation process of the $DE/rand/1/bin$, which makes to get out of local minima that do not provide promising solutions, i.e., the $DE/rand/1/bin$ performs better exploration of the search space. With the above, it is possible to observe that with the algorithm $DE/best/1/bin$, promising solutions can be reached in a wider range of values of CR, with the inconvenience that, on average, the solutions do not present a convergence towards the best individual, so it will require the execution of several runs to provide the best result. On the other hand, although the algorithm $DE/rand/1/bin$ has a smaller number of values of CR with which promising solutions are found, it will find, on average promising solutions through the algorithm executions.
- The infeasible solutions (see IS column) found through the thirty executions per sample shows that the algorithm $DE/rand/1/bin$ in thirteen cases with different values of CR, in at least one of the thirty executions, was not possible to find feasible individuals. In contrast, in five cases, the algorithm $DE/best/1/bin$ finds at least one infeasible individual in the thirty executions. This implies that the $DE/best/1/bin$ is more reliable in finding feasible solutions for this particular case.

On the other hand, nonparametric inferential statistics is used to confirm the confidence in the number of times that one algorithm outperforms the others based on their performances through a multiple comparison test [97]. The multiple comparison Friedman test is first used to detect if at least two samples have different mean values. The obtained p-value is $6.2631e-162$ indicating the existence of significant differences among the performances of the forty compared algorithms (the two DE variants with different CR values).

The Bonferroni multiple comparison post hoc test with a significance level of $\alpha = 0.05$ is also used to confirm that the medians of the data set are significantly different. The obtained p-value at each comparison is adjusted by taking into account the accumulated error in the data set of the compared algorithms. Fig. 12 displays the multiple comparison test. Lines that are overlapped mean that the algorithms are not significantly different, i.e., the p-values in those comparisons are higher than the selected significance level, and no conclusion about the data distributions can be drawn. On the contrary, algorithms with significantly different among them, present lines do not overlap, i.e., the p-value is inferior to the selected significance level, and the winner between the two algorithms is the one that is further to the left side according to the ranks. So, in this case, the stronger the evidence for accepting the alternative hypothesis is confirmed (the medians of the data set are not the same, indicating different distributions between the algorithms). In addition, in Fig. 11(a) and Fig. 11(b), the comparison of two target algorithms with respect to the rest of the algorithms is presented. The target algorithms are the two most outstanding ones for each variant. The red lines indicate significantly different algorithms, and the gray lines indicate those that are not significantly different with respect to the target algorithm shown in the blue line. This test provides the following findings:

- The comparison of the DE/rand/1/bin with $CR = 0.95$ (indicating in blue line) with respect to all algorithms is shown in Fig. 11(a). It is confirmed that DE/rand/1/bin with $CR = 0.95$ is the best option to solve the mechanism synthesis problem because this algorithm outperforms twenty-two DE variants using different CR values. Also, this algorithm provides the best objective function value.
- The comparison of DE/best/1/bin using $CR = 0.75$ with respect to all algorithms (as shown in Fig. 11(b)) indicates that this algorithm is the second best one because it outperforms eighteen algorithms using different CR values. Also, it provides a close solution ($1.2702e-4$) to the best-found solution with DE/best/1/bin using $CR = 0.80$ ($1.2034e-4$).
- It is confirmed that the variations of the crossover values in the DE/rand/1/bin present more significant differences among the comparisons than the DE/best/1/bin. Meanwhile, the DE/best/1/bin presents, in the majority of the cases, no conclusion (significance differences) about the algorithm performance with different crossover values. This is observed by visualizing the diverse set of intervals of ranks (lines).

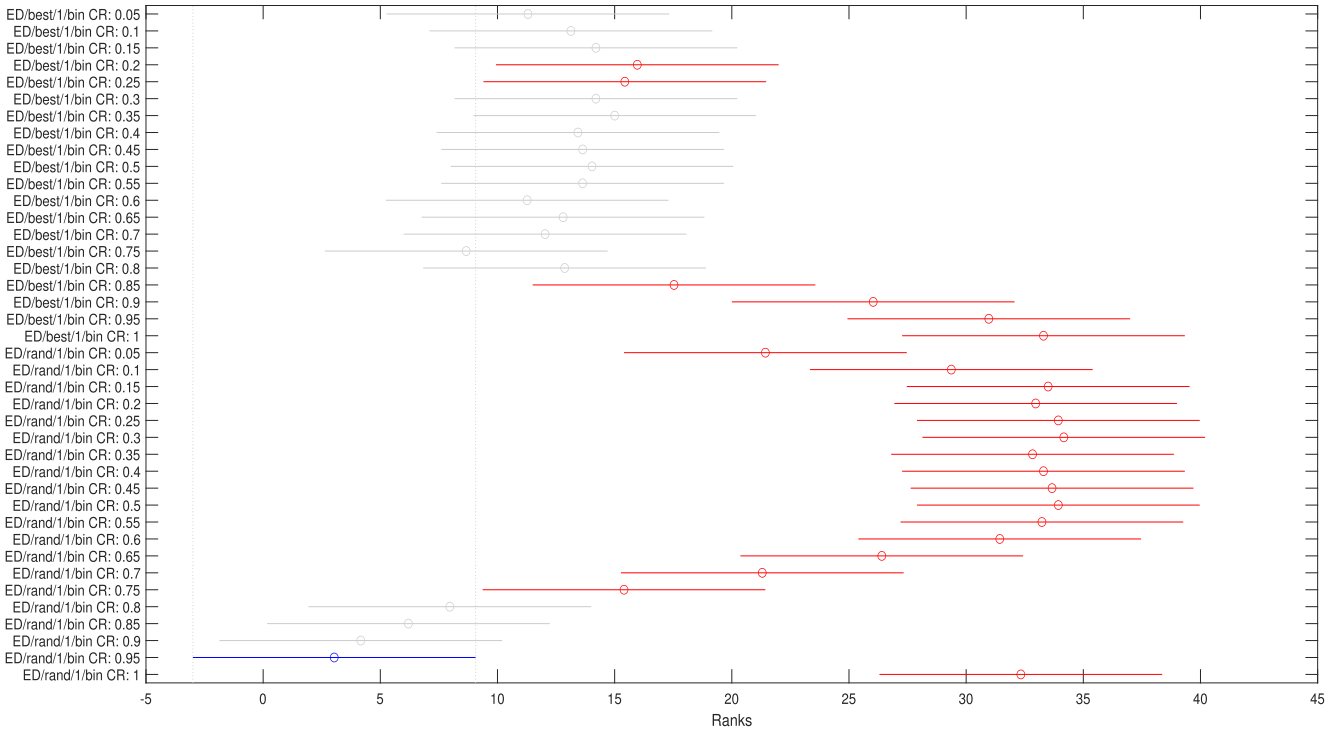

(a) Twenty-two algorithms with different CR values have average rankings that are significantly different from DE/rand/1/bin with $CR = 0.95$.

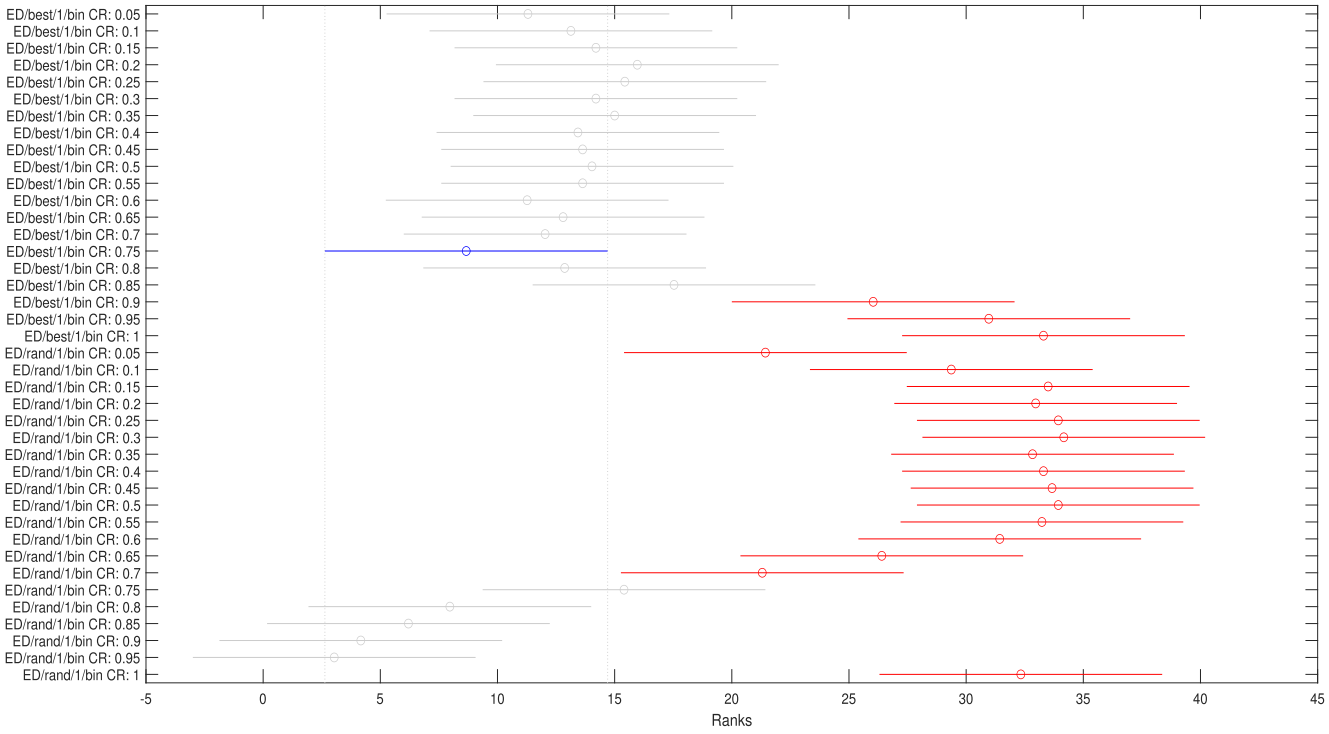

(b) Eighteen algorithms with different CR values have average rankings that are significantly different from DE/best/1/bin with $CR = 0.75$.

FIGURE 11. The Bonferroni multiple comparison post hoc test with a significance level of $\alpha = 0.05$.

Figure 12(a) shows the objective function evolution through generations of the best solution for both DE variants. It is observed in Fig. 12 for $DE/rand/1/bin$ that after the solution is feasible (around the generation 900), a decreasing trend is observed until the generation 5000. After the generation 5000, the trend is towards a certain value. In the

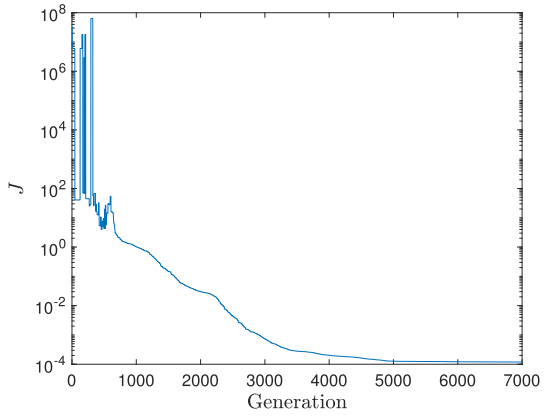

(a) $DE/rand/1/bin$ with $CR = 0.95$.

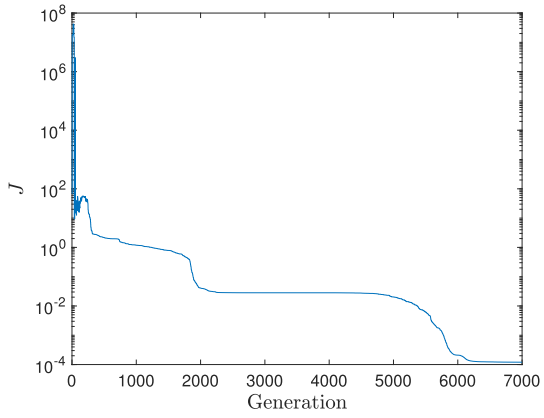

(b) $DE/best/1/bin$ with $CR = 0.8$.

FIGURE 12. Objective function behavior of the best solution found in the thirty executions.

case of $DE/best/1/bin$ showed in Fig. 12(b), the feasible solution is found in around the generation 300. After that generation, a stagnation to a local solution is observed in the interval of generations [2000, 5000]. It is also observed that the objective function evolution remains almost constant after the generation 6000. In contrast to the $DE/best/1/bin$, the behavior of the performance function in the $DE/rand/1/bin$ empirically confirms the capacity of the algorithm to go out of local solutions.

B. PERFORMANCE ANALYSIS OF THE OBTAINED SOLUTIONS

This section presents the comparative analysis of the best solutions found by the DE variants for the spherical mechanism in passive ankle rehabilitation. Table 6 shows the values of the design variables of the best solution found for both algorithms. The solution given by $DE/rand/1/bin$ obtains the best objective function value with $J = 1.1929e-4$. In the case of $DE/best/1/bin$, it has an objective function value of $J = 1.2034e-4$. The Pearson correlation coefficient between the design variables is 0.5407, which implies that there is not a relationship between both solutions in spite of having a percentage difference of 0.87% between both objective function values. Nevertheless, suppose the design

TABLE 6. Design variables found by optimizers.

Design variables	$DE/rand/1/bin$	$DE/best/1/bin$
$\bar{a}_{0x}$	-0.4746	-0.3346
$\bar{a}_{0y}$	-0.0989	-0.0695
$\bar{a}_{0z}$	-0.0117	-0.0137
$\bar{b}_{0x}$	-0.3714	-0.9999
$\bar{b}_{0y}$	0.0132	0.0393
$\bar{b}_{0z}$	-0.1531	-0.4295
$\bar{f}_x$	-0.3686	-0.1255
$\bar{f}_y$	0.5810	0.1998
$\bar{f}_z$	0.1669	0.0558
$\bar{s}_x$	0.3501	0.0522
$\bar{s}_y$	0.4289	0.0597
$\bar{s}_z$	-0.9770	-0.1516
$\bar{p}_{0x}$	0.6158	0.9799
$\bar{p}_{0y}$	-0.1638	-0.2605
$\bar{p}_{0z}$	0.2339	0.3723
θ_1	4.1817	0.7259
θ_2	4.4559	1.1291
θ_3	4.6967	1.5373
θ_5	5.0700	2.3433
θ_6	5.2373	2.7516
θ_7	5.4388	3.1538
θ_8	5.6863	3.5306
θ_9	5.9694	3.8717
θ_{10}	6.2830	4.1782
θ_{11}	5.6343e-5	4.4527
θ_{12}	0.3466	4.6936
θ_{13}	0.7265	4.8965
θ_{14}	1.1302	5.0669
θ_{15}	1.5393	5.2346
θ_{16}	1.9428	5.4367
θ_{17}	2.3462	5.6852
θ_{18}	2.7545	5.9690
θ_{19}	3.1573	6.2828
θ_{20}	3.5343	1.2734e-5
θ_{21}	3.8754	0.3461
J	**1.1929e-4**	**1.2034e-4**

variables associated with the vector coordinates are normalized according to (25)-(28). In that case, the Pearson correlation coefficient between the obtained solutions given by DE variants presents a value of 0.9998, indicating that the best mechanisms found with both algorithms have a close relationship between them. The normalized design variables (Cartesian coordinates of the spherical mechanism) are displayed in Table 7.

Table 8 shows the precision points $\boldsymbol{q}_j$, and those generated by the coupler point $\boldsymbol{p}_j$ of the best mechanism found with the $DE/rand/1/bin$. The positions of those points are graphically observed in Fig. 13, where red circles represent the precision points, and blue crosses are the coupler points of the mechanism through diverse movements of the mechanism's crank. Moreover, in Fig. 13(c) a close-up view of

TABLE 7. Cartesian coordinates of both the mechanism joints and the coupler point.

Coordinates	$DE/rand/1/bin$	$DE/best/1/bin$
a_{0x}	-0.9240	-0.9182
a_{0y}	0.0329	0.0360
a_{0z}	-0.3809	-0.3944
b_{0x}	0.3117	0.3052
b_{0y}	0.3819	0.3490
b_{0z}	-0.8700	-0.8860
f_x	-0.9786	-0.9782
f_y	-0.2041	-0.2034
f_z	-0.0243	-0.04021
s_x	-0.5206	-0.5174
s_y	0.8205	0.8241
s_z	0.2357	0.2300
p_{0x}	0.9071	0.9071
p_{0y}	-0.2413	-0.2411
p_{0z}	0.3446	0.3447
J	**1.1929e-4**	**1.2034e-4**

TABLE 8. Coordinates for the precision points and the obtained coordinates in the coupler point of the spherical mechanism.

	$\boldsymbol{q}_j$			$\boldsymbol{p}_j$		
j	q_{j_x}	q_{j_y}	q_{j_z}	p_{j_x}	p_{j_y}	p_{j_z}
1	0.9063	-0.2423	0.3461	0.9071	-0.2413	0.3446
2	0.9059	-0.1114	0.4083	0.9065	-0.1110	0.4071
3	0.9048	0.0470	0.4231	0.9041	0.0471	0.4245
4	0.9032	0.2078	0.3754	0.9022	0.2088	0.3772
5	0.9027	0.3382	0.2658	0.9029	0.3379	0.2655
6	0.9054	0.4093	0.1122	0.9064	0.4071	0.1118
7	0.9123	0.4056	-0.0550	0.9125	0.4052	-0.0549
8	0.9219	0.3302	-0.2023	0.9210	0.3319	-0.2038
9	0.9311	0.2031	-0.3027	0.9306	0.2037	-0.3040
10	0.9374	0.0541	-0.3437	0.9381	0.0540	-0.3419
11	0.9396	-0.0885	-0.3303	0.9407	-0.0877	-0.3274
12	0.9374	-0.2069	-0.2797	0.9376	-0.2068	-0.2794
13	0.9311	-0.2961	-0.2126	0.9299	-0.2982	-0.2151
14	0.9219	-0.3588	-0.1457	0.9206	-0.3613	-0.1478
15	0.9123	-0.4000	-0.0870	0.9126	-0.3993	-0.0866
16	0.905	-0.4230	-0.0344	0.9072	-0.41922	-0.0333
17	0.9027	-0.4297	0.0204	0.9038	-0.4274	0.0205
18	0.9032	-0.4203	0.0866	0.9022	-0.4223	0.08701
19	0.9048	-0.3912	0.1677	0.9031	-0.3944	0.1693
20	0.9059	-0.3348	0.2589	0.9055	-0.3355	0.2595
21	0.9063	-0.2423	0.3461	0.9071	-0.2413	0.3446

a point is observed. The average distance value from the precision and coupler points shown in Table 8 is 0.00209, with a maximum distance value of 0.00437 and a minimum one of $3.62047e-4$. So, the spherical mechanism can follow the desired path with a percentage error in the interval $[0.437, 0.036]\%$.

On the other hand, the graphical representation of the spherical mechanism through four different rotations of

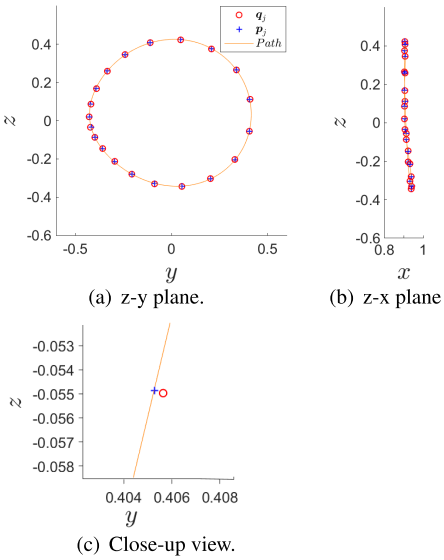

FIGURE 13. Path, coupler and precision points generated by the spherical mechanism.

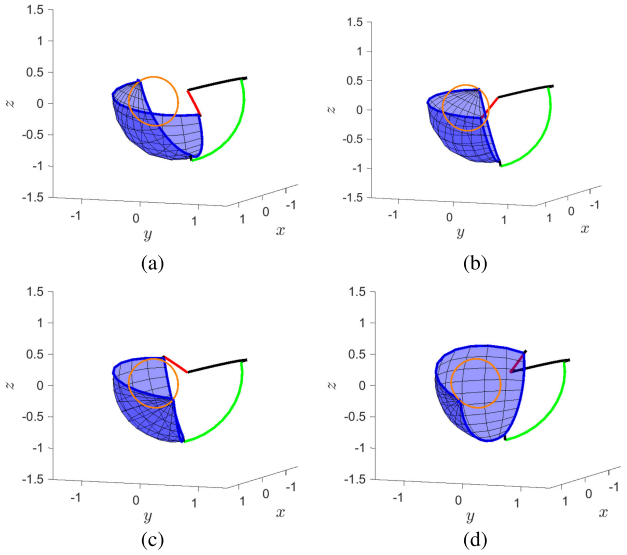

FIGURE 14. Graphical representation of the crank movement of spherical mechanism.

the crank (red link) in a simulation environment is shown in Fig. 14. The black link represents the ground link, the green link is the output (rocker) link, and the spherical triangle (blue link) represents the coupler link. It is observed that the coupler point describes the desired path.

C. EXPERIMENTAL PROTOTYPE

The obtained numerical results are validated by manufacturing the ankle rehabilitation mechanism with a 3D printer. Figure 15 shows the experimental prototype and the Computer-Aided Design (CAD) of the obtained design. The red, black, green, and blue links in Fig. 15(b) represent the crank (r_2), ground (r_1), rocker (r_4), and coupler links (r_3), respectively.

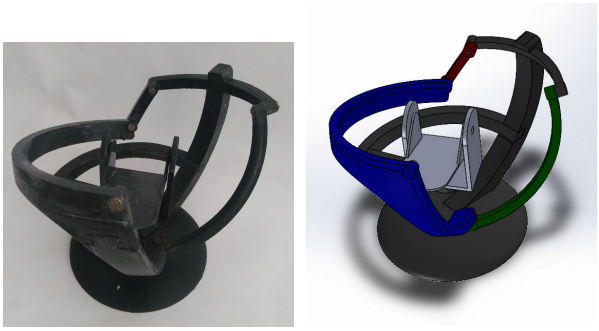

(a) Manufactured prototype. (b) CAD model.

FIGURE 15. Spherical mechanism prototype for passive ankle rehabilitation.

TABLE 9. Geodesic distance of the manufactured prototype.

Link	Geodesic distance with unit radius	Scale factor [mm]	Geodesic distance with scaling [mm]
r_1	1.2278	72+10=83	101.91
r_2	0.4352	72+5=77	33.51
r_3	1.5148	72	109.06
r_4	1.6248	72+5=77	125.10
r_5	2.9284	72	210.84

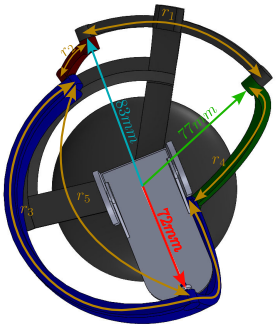

FIGURE 16. Radial distances of the sphere layer that contains links.

Also, the base where the foot should rest is displayed in gray color. As the coordinates of the spherical mechanism links are expressed in unit vectors (an sphere with unit radius), the obtained geodesic distances also represent the arc angles, and those distances must change to manufacture the prototype. Therefore, the size of the geodesic distances is enlarged by multiplying the obtained arc angle by a scale factor to allow links with different geodesic distances to be assembled. The scale factor represents a new radius of the sphere related to the foot size, with or without the addition of the link width. The scale factors and the resulting geodesic distances are presented in Table 9, where r_5 is the geodesic distance joining the points $\boldsymbol{a}_0$ and $\boldsymbol{p}_0$.

The detailed description for generating the scale factor is explained next using Fig. 16: In this case the prototype is scaled 30% from the original size. It is considered that the foot size is 240 mm, so the scaled foot size is 72 mm.

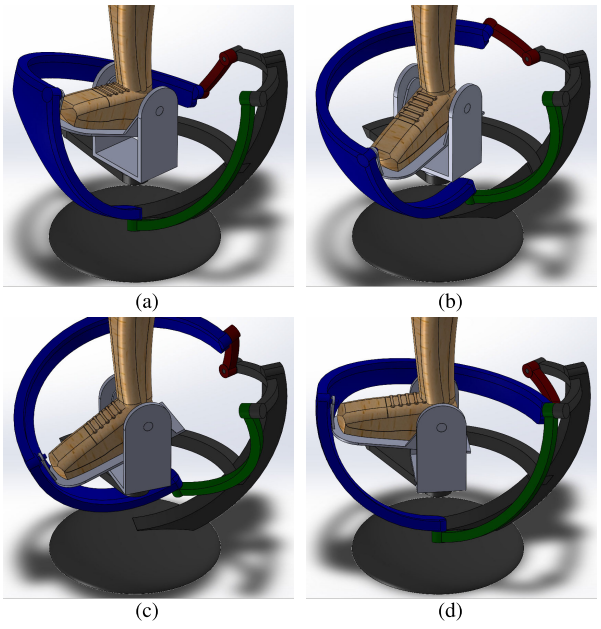

(a) (b) (c) (d)

FIGURE 17. Motion simulation in the CAD of the spherical mechanism for passive ankle rehabilitation. For more details see the video in this link (click here).

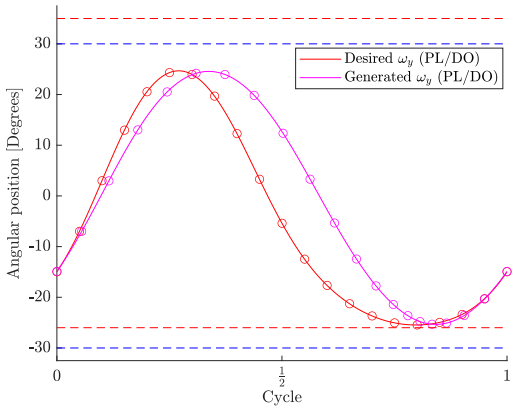

(a) Plantarflexion/dorsiflexion movement.

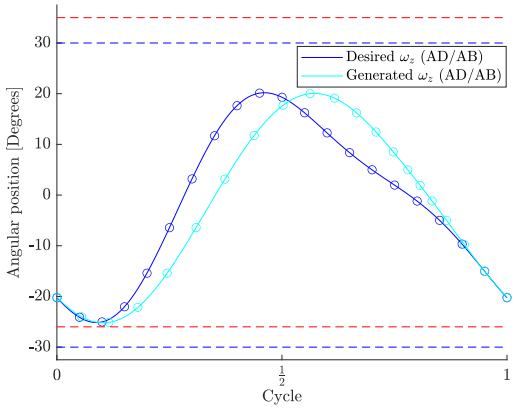

(b) Adduction/abduction movement.

FIGURE 18. Angular displacement in the spherical joint.

This scaled foot size represents the radius of the sphere layer that contains the geodesic distances r_3 and r_5. The following exterior sphere layer has an increment related to the link

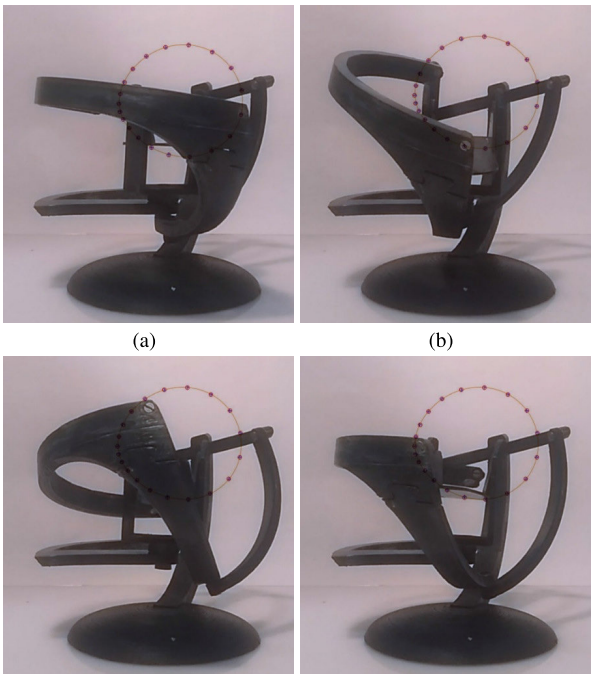

FIGURE 19. Path following of the passive ankle rehabilitation prototype.

width (5 mm), and this layer contains the geodesic distances r_2 and r_4. The last layer contains the geodesic distance r_1, which represents an increment of two times the link width with respect to the scaled foot size.

Figure 17 shows the motion simulation of the rehabilitation mechanism in four different positions in the CAD model. The corresponding angular position of the PL/DO and the AD/AB movements of the ankle (spherical joint) are displayed in Fig. 18. It is observed that the precision points transformed into the angular space present the minimum and maximum errors of 0.0127 and 0.2435 degrees in the PL/DO movement, respectively. In a similar fashion those errors in the AD/AB movement are $5.8031e{-}4$ and 0.1775 degrees. These values additionally confirm the precision to perform the rehabilitation trajectory by using the obtained rehabilitation mechanism.

Finally, the movement of the prototype of the ankle rehabilitation mechanism is exposed in four photographs given in Fig. 19, and also a video of the prototype functionality is given in this link (click here). It is observed that the experimental prototype fulfills the desired path for ankle rehabilitation.

VI. CONCLUSION

This paper presents the design approach of an ankle rehabilitation device with a one-degree-of-freedom spherical mechanism through an optimization approach. The proposed design is formulated as a mono-objective constraint optimization problem where the relative angle approach, the Grashof criterion, the force transmission and the rehabilitation routine are included in the dimensional synthesis to find the link-Cartesian coordinates that perform a passive rehabilitation exercise. The resulting design is obtained through differential evolution variants $DE/rand/1/bin$ and $DE/best/1/bin$.

The statistical results using the differential evolution variants indicate that both algorithms find similar solutions with a slight difference of 0.87% in the objective function value given by $DE/rand/1/bin$ than the provided by the $DE/best/1/bin$. Also, the Pearson correlation coefficient confirms the close relationship of 0.9998 in the obtained design solutions. Considering that the CR value is the only parameter configuration of the algorithms and it must choose in the interval [0, 1], the $DE/best/1/bin$ can reach promising solutions in 45% of the interval. In contrast, the $DE/rand/1/bin$ can reach them in 15%. This indicates that the algorithm's parameter configuration is more critical in $DE/rand/1/bin$, because the $DE/best/1/bin$ can reach promising solutions in a wider range of CR values than $DE/rand/1/bin$. On the other hand, several executions of the algorithms are required to provide the best solution to the problem in both algorithms. In those executions, there also exist solutions that do not converge to the best solution region. This fact is attributed to the way of stating the optimization problem, i.e., the inclusion of the relative angle approach in the dimensional synthesis. This is because this approach can search in a broader field of the search space, so there is more chance to converge to local solutions to the problem. Future work involves the improvement of the optimizer to make a better balance in the exploration and exploitation of the search space, such that the convergence of the algorithm to the best solution region is more reliable through the executions in this kind of kinematic synthesis problem statement.

The numerical simulation results, the motion simulation of the CAD model, and the ankle rehabilitation mechanism prototype show the movement of the final design where the percentage error between the desired rehabilitation path and the curve generated by the coupler point of the mechanism is in the interval [0.036, 0.437]% with an average error of 0.209%. So, the potential of the proposed rehabilitation mechanism is evidenced as an aid in developing passive ankle rehabilitation exercises. Future work will also concern experimentally testing the device and designing additional devices with the proposed approach to carrying out rehabilitation exercises.

The proposed nature-inspired intelligent synthesis design methodology can be extended for coupling spherical four-bar mechanisms to generate more complex paths. Other future work involves including the eversion/inversion ankle movement into the nature-inspired intelligent synthesis through coupling mechanisms.

REFERENCES

[1] M. Dong, Y. Zhou, J. Li, X. Rong, W. Fan, X. Zhou, and Y. Kong, "State of the art in parallel ankle rehabilitation robot: A systematic review," *J. NeuroEng. Rehabil.*, vol. 18, no. 1, pp. 1–15, Mar. 2021.

[2] P. Capodaglio, M. Gobbi, L. Donno, A. Fumagalli, C. Buratto, M. Galli, and V. Cimolin, "Effect of obesity on knee and ankle biomechanics during walking," *Sensors*, vol. 21, no. 21, pp. 1–11, 2021.

[3] M. Cilli, K. Serbest, and E. Kayaoglu, "The effect of body weight on joint torques in teenagers: Investigation of sit-to-stand movement," *Clin. Biomechanics*, vol. 83, Mar. 2021, Art. no. 105288.
[4] E. R. Barill and D. A. Porter, "principles of rehabilitation for the foot and ankle," in *Baxter's the Foot and Ankle in Sport*, 2nd ed., D. A. Porter and L. C. Schon, Eds. Philadelphia, PA, USA: Mosby, 2008, pp. 595–610.
[5] M. De Noronha, E. K. Lay, M. R. Mcphee, G. Mnatzaganian, and G. S. Nunes, "Ankle sprain has higher occurrence during the latter parts of matches: Systematic review with meta-analysis," *J. Sport Rehabil.*, vol. 28, no. 4, pp. 373–380, May 2019.
[6] P. J. O'Neill, B. G. Parks, R. Walsh, L. M. Simmons, and S. D. Miller, "Excursion and strain of the superficial peroneal nerve during inversion ankle sprain," *J. Bone Joint Surgery*, vol. 89, no. 5, pp. 979–986, May 2007.
[7] T. Bestwick-Stevenson, L. A. Wyatt, D. Palmer, A. Ching, R. Kerslake, F. Coffey, M. E. Batt, and B. E. Scammell, "Incidence and risk factors for poor ankle functional recovery, and the development and progression of posttraumatic ankle osteoarthritis after significant ankle ligament injury (SALI): The SALI cohort study protocol," *BMC Musculoskeletal Disorders*, vol. 22, no. 1, p. 362, Dec. 2021.
[8] B. Dasgupta and T. S. Mruthyunjaya, "The stewart platform manipulator: A review," *Mechanism Mach. Theory*, vol. 35, no. 1, pp. 15–40, Jan. 2000.
[9] M. J. Girone, G. C. Burdea, and M. Bouzit, "The 'Rutgers Ankle' orthopedic rehabilitation interface," in *Dynamic Systems and Control* (ASME International Mechanical Engineering Congress and Exposition). Little Falls, NJ, USA: The ASME Digital Collection, Nov. 1999, pp. 305–312.
[10] G. Liu, J. Gao, H. Yue, X. Zhang, and G. Lu, "Design and kinematics analysis of parallel robots for ankle rehabilitation," in *Proc. IEEE/RSJ Int. Conf. Intell. Robots Syst.*, Oct. 2006, pp. 253–258.
[11] J. A. Saglia, N. G. Tsagarakis, J. S. Dai, and D. G. Caldwell, "Inverse-kinematics-based control of a redundantly actuated platform for rehabilitation," *Proc. Inst. Mech. Eng., I, J. Syst. Control Eng.*, vol. 223, no. 1, pp. 53–70, Feb. 2009.
[12] J. S. Dai, T. Zhao, and C. Nester, "Sprained ankle physiotherapy based mechanism synthesis and stiffness analysis of a robotic rehabilitation device," *Auto. Robots*, vol. 16, no. 2, pp. 207–218, Mar. 2004.
[13] Q. Liu, J. Zuo, C. Zhu, W. Meng, Q. Ai, and S. Q. Xie, "Design and hierarchical force-position control of redundant pneumatic muscles-cable-driven ankle rehabilitation robot," *IEEE Robot. Autom. Lett.*, vol. 7, no. 1, pp. 502–509, Jan. 2022.
[14] J. Kwon, J. Park, S. Ku, Y. Jeong, N. Paik, and Y. Park, "A soft wearable robotic ankle-foot-orthosis for post-stroke patients," *IEEE Robot. Autom. Lett.*, vol. 4, no. 3, pp. 2547–2552, Jul. 2019.
[15] M. Hassan and A. Khajepour, "Analysis of bounded cable tensions in cable-actuated parallel manipulators," *IEEE Trans. Robot.*, vol. 27, no. 5, pp. 891–900, Oct. 2011.
[16] J. Zhang, C. Liu, T. Liu, K. Qi, J. Niu, and S. Guo, "Module combination based configuration synthesis and kinematic analysis of generalized spherical parallel mechanism for ankle rehabilitation," *Mechanism Mach. Theory*, vol. 166, Dec. 2021, Art. no. 104436.
[17] L. Zhang, J. Li, M. Dong, B. Fang, Y. Cui, S. Zuo, and K. Zhang, "Design and workspace analysis of a parallel ankle rehabilitation robot (PARR)," *J. Healthcare Eng.*, vol. 2019, Mar. 2019, Art. no. 4164790.
[18] P. Sui, L. Yao, Z. Lin, H. Yan, and J. S. Dai, "Analysis and synthesis of ankle motion and rehabilitation robots," in *Proc. IEEE Int. Conf. Robot. Biomimetics (ROBIO)*, Dec. 2009, pp. 2533–2538.
[19] M. Malosio, S. P. Negri, N. Pedrocchi, F. Vicentini, M. Caimmi, and L. M. Tosatti, "A spherical parallel three degrees-of-freedom robot for ankle-foot neuro-rehabilitation," in *Proc. Annu. Int. Conf. IEEE Eng. Med. Biol. Soc.*, Aug. 2012, pp. 3356–3359.
[20] C. M. Gosselin, E. S. Pierre, and M. Gagne, "On the development of the Agile Eye," *IEEE Robot. Autom. Mag.*, vol. 3, no. 4, pp. 29–37, Dec. 1996.
[21] I. Doroftei, C. M. Racu, C. Honceriu, and D. Irimia, "A one-degree-of freedom ankle rehabilitation platform," in *Proc. IOP Conf. Mater. Sci. Eng.*, Aug. 2019, vol. 591, no. 1, Art. no. 012076.
[22] M. G. Villarreal-Cervantes, J. S. Pantoja-García, A. Rodríguez-Molina, and S. E. Benitez-Garcia, "Pareto optimal synthesis of eight-bar mechanism using meta-heuristic multi-objective search approaches: Application to bipedal gait generation," *Int. J. Syst. Sci.*, vol. 52, no. 4, pp. 1–23, 2020.
[23] L. E. Valencia-Segura, M. G. Villarreal-Cervantes, L. G. Corona-Ramírez, F. Cuenca-Jiménez, and R. Castro-Medina, "Optimum synthesis of four-bar mechanism by using relative angle method: A comparative performance study," *IEEE Access*, vol. 9, pp. 132990–133010, 2021.
[24] Q. Huang, Y. Yu, K. Zhang, S. Li, H. Lu, J. Li, A. Zhang, and T. Mei, "Optimal synthesis of mechanisms using repellency evolutionary algorithm," *Knowl.-Based Syst.*, vol. 239, Mar. 2022, Art. no. 107928.
[25] J. J. Uicker, G. Pennock, and J. E. Shigley, *Theory of Machines and Mechanisms*. New York, NY, USA: Oxford Univ. Press, 2010.
[26] R. L. Norton, *Design of Machinery: An Introduction to the Synthesis And Analysis of Mechanisms And Machines*. Boston, MA, USA: McGraw-Hill Higher Education, 2004.
[27] R. Kraus, "Wertigkeitsbilanz und ihre Anwendung auf eine Geradführung für Meβ3geräte," *Feinwerktechnik*, vol. 56, no. 3, pp. 57–63, 1952.
[28] Z. Liu and J. Angeles, "Least-square optimization of planar and spherical four-bar function generator under mobility constraints," *J. Mech. Design*, vol. 114, no. 4, pp. 569–573, Dec. 1992, doi: 10.1115/1.2917045.
[29] J. Angeles and Z. Liu, "The constrained least-square optimization of spherical four-bar path generators," *J. Mech. Des.*, vol. 114, no. 3, pp. 394–405, Sep. 1992, doi: 10.1115/1.2926565.
[30] W.-T. Lee, K. Russell, Q. Shen, and R. S. Sodhi, "On adjustable spherical four-bar motion generation for expanded prescribed positions," *Mechanism Mach. Theory*, vol. 44, no. 1, pp. 247–254, Jan. 2009. [Online]. Available: https://www.sciencedirect.com/science/article/pii/S0094114X08000256
[31] J. Sun, L. Chen, and J. Chu, "Motion generation of spherical four-bar mechanism using harmonic characteristic parameters," *Mechanism Mach. Theory*, vol. 95, pp. 76–92, Jan. 2016. [Online]. Available: https://www.sciencedirect.com/science/article/pii/S0094114X15002050
[32] J. Chu and J. Sun, "Numerical atlas method for path generation of spherical four-bar mechanism," *Mechanism Mach. Theory*, vol. 45, no. 6, pp. 867–879, Jun. 2010. [Online]. Available: https://www.sciencedirect.com/science/article/pii/S0094114X09002286
[33] N. Siddique and H. Adeli, "Nature inspired computing: An overview and some future directions," *Cognit. Comput.*, vol. 7, no. 6, pp. 706–714, Dec. 2015.
[34] K. Price, R. M. Storn, and J. A. Lampinen, *Differential Evolution: A Practical Approach to Global Optimization*. Berlin, Germany: Springer, 2006.
[35] J. Holland, *Adaptation in Natural and Artificial Systems*. Cambridge, MA, USA: MIT Press, 1992.
[36] J. Kennedy and R. Eberhart, "Particle swarm optimization," in *Proc. IEEE ICNN*, vol. 4. Nov./Dec. 1995, pp. 1942–1948.
[37] S. Das and P. N. Suganthan, "Differential evolution: A survey of the state-of-the-art," *IEEE Trans. Evol. Comput.*, vol. 15, no. 1, pp. 4–31, Feb. 2011.
[38] M. F. Ahmad, N. A. M. Isa, W. H. Lim, and K. M. Ang, "Differential evolution: A recent review based on state-of-the-art works," *Alexandria Eng. J.*, vol. 61, no. 5, pp. 3831–3872, May 2022. [Online]. Available: https://www.sciencedirect.com/science/article/pii/S111001682100613X
[39] Bilal, M. Pant, H. Zaheer, L. Garcia-Hernandez, and A. Abraham, "Differential evolution: A review of more than two decades of research," *Eng. Appl. Artif. Intell.*, vol. 90, Apr. 2020, Art. no. 103479. [Online]. Available: https://www.sciencedirect.com/science/article/pii/S095219762030004X
[40] F. Peñuñuri, R. Peón-Escalante, C. Villanueva, and C. A. Cruz-Villar, "Synthesis of spherical 4R mechanism for path generation using differential evolution," *Mechanism Mach. Theory*, vol. 57, pp. 62–70, Nov. 2012. [Online]. Available: https://www.sciencedirect.com/science/article/pii/S0094114X12001450
[41] G. P. Roston and R. H. Sturges, "Genetic algorithm synthesis of four-bar mechanisms," *Artif. Intell. Eng. Design, Anal. Manuf.*, vol. 10, no. 5, pp. 371–390, Nov. 1996.
[42] S. Datoussaïd, O. Verlinden, and C. Conti, "Optimal design of multibody systems by using genetic algorithms," *Vehicle Syst. Dyn.*, vol. 29, no. S1, pp. 704–710, 1998.
[43] J. A. Cabrera, A. Simon, and M. Prado, "Optimal synthesis of mechanisms with genetic algorithms," *Mechanism Mach. Theory*, vol. 37, no. 10, pp. 1165–1177, Oct. 2002.
[44] J. A. Cabrera, F. Nadal, J. P. Muñoz, and A. Simon, "Multiobjective constrained optimal synthesis of planar mechanisms using a new evolutionary algorithm," *Mechanism Mach. Theory*, vol. 42, no. 7, pp. 791–806, Jul. 2007.
[45] P. S. Shiakolas, D. Koladiya, and J. Kebrle, "On the optimum synthesis of four-bar linkages using differential evolution and the geometric centroid of precision positions," *Inverse Problems Eng.*, vol. 10, no. 6, pp. 485–502, Jan. 2002.

[46] R. R. Bulatović and S. R. Dordević, "On the optimum synthesis of a four-bar linkage using differential evolution and method of variable controlled deviations," *Mechanism Mach. Theory*, vol. 44, no. 1, pp. 235–246, Jan. 2009.

[47] P. S. Shiakolas, D. Koladiya, and J. Kebrle, "On the optimum synthesis of six-bar linkages using differential evolution and the geometric centroid of precision positions technique," *Mechanism Mach. Theory*, vol. 40, no. 3, pp. 319–335, Mar. 2005.

[48] M. Laribi, L. Romdhane, A. Mlika, and S. Zeghloul, "A combined genetic algorithm-fuzzy logic method (GA-FL) to design a 6 bars planar mechanism," in *Proc. ASME 7th Biennial Conf. Eng. Syst. Design Anal.*, vol. 41731. Little Falls, NJ, USA: The ASME Digital Collection, 2004, pp. 733–738.

[49] J. A. Cabrera, A. Ortiz, F. Nadal, and J. J. Castillo, "An evolutionary algorithm for path synthesis of mechanisms," *Mechanism Mach. Theory*, vol. 46, no. 2, pp. 127–141, Feb. 2011.

[50] S. Ebrahimi and P. Payvandy, "Efficient constrained synthesis of path generating four-bar mechanisms based on the heuristic optimization algorithms," *Mechanism Mach. Theory*, vol. 85, pp. 189–204, Mar. 2015.

[51] S. K. Acharyya and M. Mandal, "Performance of EAs for four-bar linkage synthesis," *Mechanism Mach. Theory*, vol. 44, no. 9, pp. 1784–1794, Sep. 2009.

[52] A. Smaili and N. Diab, "Optimum synthesis of hybrid-task mechanisms using ant-gradient search method," *Mechanism Mach. Theory*, vol. 42, no. 1, pp. 115–130, Jan. 2007.

[53] W.-Y. Lin, "A GA–DE hybrid evolutionary algorithm for path synthesis of four-bar linkage," *Mechanism Mach. Theory*, vol. 45, no. 8, pp. 1096–1107, Aug. 2010.

[54] R. R. Bulatovic, S. R. Dordevic, and V. S. Dordevic, "Cuckoo search algorithm: A metaheuristic approach to solving the problem of optimum synthesis of a six-bar double dwell linkage," *Mechanism Mach. Theory*, vol. 61, pp. 1–13, Mar. 2013.

[55] E. Badreddine, A. Houidi, Z. Affi, and L. Romdhane, "Application of multi-objective genetic algorithms to the mechatronic design of a four bar system with continuous and discrete variables," *Mechanism Mach. Theory*, vol. 61, pp. 68–83, 2013.

[56] R. R. Bulatović, G. Miodragović, and M. S. Bošković, "Modified Krill Herd (MKH) algorithm and its application in dimensional synthesis of a four-bar linkage," *Mechanism Mach. Theory*, vol. 95, pp. 1–21, Jan. 2016.

[57] R. Singh, H. Chaudhary, and A. K. Singh, "Defect-free optimal synthesis of Crank–Rocker linkage using nature-inspired optimization algorithms," *Mechanism Mach. Theory*, vol. 116, pp. 105–122, Oct. 2017.

[58] K. Zhang, Q. Huang, Y. Zhang, J. Song, and J. Shi, "Hybrid Lagrange interpolation differential evolution algorithm for path synthesis," *Mechanism Mach. Theory*, vol. 134, pp. 512–540, Apr. 2019.

[59] R. Sancibrian, A. Sedano, E. G. Sarabia, and J. M. Blanco, "Hybridizing differential evolution and local search optimization for dimensional synthesis of linkages," *Mechanism Mach. Theory*, vol. 140, pp. 389–412, Oct. 2019.

[60] W.-Y. Lin and K.-M. Hsiao, "Cuckoo search and teaching–learning-based optimization algorithms for optimum synthesis of path-generating four-bar mechanisms," *J. Chin. Inst. Eng.*, vol. 40, no. 1, pp. 66–74, Jan. 2017.

[61] S. Nguyen-Van, Q. X. Lieu, N. Xuan-Mung, and T. T. N. Nguyen, "A new study on optimization of four-bar mechanisms based on a hybrid-combined differential evolution and Jaya algorithm," *Symmetry*, vol. 14, no. 2, p. 381, Feb. 2022.

[62] S. Sleesongsom and S. Bureerat, "Four-bar linkage path generation through self-adaptive population size teaching-learning based optimization," *Knowl.-Based Syst.*, vol. 135, pp. 180–191, Nov. 2017.

[63] N. Eqra, A. H. Abiri, and R. Vatankhah, "Optimal synthesis of a four-bar linkage for path generation using adaptive PSO," *J. Brazilian Soc. Mech. Sci. Eng.*, vol. 40, no. 9, pp. 1–11, Sep. 2018.

[64] N. Eqra, S. Taghvaei, and R. Vatankhah, "Optimal kinematic design of a single-DOF planar grasper based on metaheuristic optimization," *J. Brazilian Soc. Mech. Sci. Eng.*, vol. 41, no. 10, pp. 1–11, Oct. 2019.

[65] M. A. Ben Abdallah, I. Khemili, and N. Aifaoui, "Flexible slider Crank mechanism synthesis using meta-heuristic optimization techniques: A new designer tool assistance for a compliant mechanism synthesis," *Artif. Intell. Rev.*, vol. 53, no. 4, pp. 2809–2840, Apr. 2020.

[66] K. Zhang, M. Yang, Y. Zhang, and Q. Huang, "Error feedback method (Efm) based dimension synthesis optimization for four-bar linkage mechanism," *SSRN Electron. J.*, vol. 1, no. 1, pp. 1–31, 2022.

[67] J. K. Mwangi, O. M. Muvengei, and M. F. Oduori, "Review of the application of genetic algorithm and precision points in optimisation of the four-bar mechanism," in *Proc. Sustain. Res. Innov. Conf.*, 2022, pp. 203–212.

[68] S. Vera and S. Prado, "Synthesis and optimization of a needles robotic gripper mechanism for transplanting seedlings," in *Proc. IEEE ANDESCON*, Oct. 2020, pp. 1–6.

[69] J.-A. Leal-Naranjo, J.-A. Soria-Alcaraz, C.-R. Torres-San Miguel, J.-C. Paredes-Rojas, A. Espinal, and H. Rostro-González, "Comparison of metaheuristic optimization algorithms for dimensional synthesis of a spherical parallel manipulator," *Mechanism Mach. Theory*, vol. 140, pp. 586–600, Oct. 2019.

[70] A. Bataller, J. A. Cabrera, M. Clavijo, and J. J. Castillo, "Evolutionary synthesis of mechanisms applied to the design of an exoskeleton for finger rehabilitation," *Mechanism Mach. Theory*, vol. 105, pp. 31–43, Nov. 2016.

[71] Y. Shao, Z. Xiang, H. Liu, and L. Li, "Conceptual design and dimensional synthesis of cam-linkage mechanisms for gait rehabilitation," *Mechanism Mach. Theory*, vol. 104, pp. 31–42, Oct. 2016.

[72] R. Singh, H. Chaudhary, and A. K. Singh, "A novel gait-based synthesis procedure for the design of 4-bar exoskeleton with natural trajectories," *J. Orthopaedic Transl.*, vol. 12, pp. 6–15, Jan. 2018.

[73] J. S. Muñoz-Reina, M. G. Villarreal-Cervantes, and L. G. Corona-Ramírez, "Integrated design of a lower limb rehabilitation mechanism using differential evolution," *Comput. Electr. Eng.*, vol. 92, Jun. 2021, Art. no. 107103.

[74] J. S. Muñoz-Reina, M. G. Villarreal-Cervantes, and L. G. Corona-Ramírez, "Empirical study of constraint-handling techniques in the optimal synthesis of mechanisms for rehabilitation," *Appl. Sci.*, vol. 11, no. 18, p. 8739, Sep. 2021.

[75] J. S. Muñoz-Reina, M. G. Villarreal-Cervantes, L. G. Corona-Ramírez, and L. E. Valencia-Segura, "Neuronal constraint-handling technique for the optimal synthesis of closed-chain mechanisms in lower limb rehabilitation," *Appl. Sci.*, vol. 12, no. 5, p. 2396, Feb. 2022.

[76] D. Chakraborty, A. Rathi, R. Singh, V. K. Pathak, K. Chaudhary, and H. Chaudhary, "Design of a stephenson III six-bar path generating mechanism for index finger rehabilitation device using nature-inspired algorithms," *Neural Comput. Appl.*, vol. 33, no. 24, pp. 17315–17329, Dec. 2021.

[77] J. Araque and G. M. Contreras, "Improvement of a mechanism to recover from knee injury by applying particle swarm optimization," *Int. J. Mech. Eng. Technol.*, vol. 10, no. 12, 2019.

[78] O. Selvi, M. Ceccarelli, and S. Yavuz, "Design and optimization of a walking over-constrained mechanism," in *Proc. IFToMM World Congr. Mechanism Mach. Sci.* Cham, Switzerland: Springer, 2019, pp. 681–687.

[79] C. H. Shu and C. W. Radcliffe, *Kinematics & Mechanisms Desing*. Hoboken, NJ, USA: Wiley, 1978.

[80] C.-H. Chiang, *Kinematics of Spherical Mechanisms*, vol. 5. Cambridge, U.K.: Cambridge Univ. Press, 1988.

[81] M. W. Spong, S. Hutchinson, and V. Mathukumalli, *Robot Modeling and Control*. Hoboken, NJ, USA: Wiley, 2020.

[82] C. H. Suh and C. W. Radcliffe, *Kinematics and Mechanisms Design*. Hoboken, NJ, USA: Wiley, 1978.

[83] A. V. Mohan Rao and G. N. Sandor, "Extension of Freudenstein's equation to geared linkages," *J. Eng. Ind.*, vol. 93, no. 1, pp. 201–210, Feb. 1971.

[84] C. A. Pickover, *The Math Book: From Pythagoras to the 57th Dimension, 250 Milestones in the History of Mathematics*. New York, NY, USA: Sterling Publishing Company, 2009.

[85] S. A. Norkus and R. Floyd, "The anatomy and mechanisms of syndesmotic ankle sprains," *J. Athletic Training*, vol. 36, no. 1, p. 68, 2001.

[86] A. Erdogan, B. Celebi, A. C. Satici, and V. Patoglu, "Assist on-ankle: A reconfigurable ankle exoskeleton with series-elastic actuation," *Auto. Robots*, vol. 41, no. 3, pp. 743–758, Mar. 2017.

[87] G. Liu, J. Gao, H. Yue, X. Zhang, and G. Lu, "Design and kinematics simulation of parallel robots for ankle rehabilitation," in *Proc. Int. Conf. Mechatronics Autom.*, 2006, pp. 1109–1113.

[88] F. Grashof, *Theoretische Maschinenlehre*, vol. 2. Hamburg, Germany: Voss, 1883.

[89] S. S. Balli and S. Chand, "Transmission angle in mechanisms (Triangle in mech)," *Mechanism Mach. Theory*, vol. 37, no. 2, pp. 175–195, Feb. 2002.

[90] M. Petrera and Y. B. Suris, "Spherical geometry and integrable systems," *Geometriae Dedicata*, vol. 169, no. 1, pp. 83–98, Apr. 2014.

[91] V. Kachitvichyanukul, "Comparison of three evolutionary algorithms: GA, PSO, and DE," *Ind. Eng. Manage. Syst.*, vol. 11, no. 3, pp. 215–223, Sep. 2012.

[92] J. Nocedal and S. Wright, *Numerical Optimization*. NY, USA: Springer, 2006.
[93] S. S. Rao, *Engineering Optimization: Theory and Practice*. Hoboken, NJ, USA: Wiley, 2019.
[94] E. Mezura-Montes and C. A. C. Coello, "Constraint-handling in nature-inspired numerical optimization: Past, present and future," *Swarm Evol. Comput.*, vol. 1, no. 4, pp. 173–194, Dec. 2011.
[95] K. Deb, "An efficient constraint handling method for genetic algorithms," *Comput. Methods Appl. Mech. Eng.*, vol. 186, nos. 2–4, pp. 311–338, Jun. 2000.
[96] C. Huang, Y. Li, and X. Yao, "A survey of automatic parameter tuning methods for metaheuristics," *IEEE Trans. Evol. Comput.*, vol. 24, no. 2, pp. 201–216, Apr. 2020.
[97] J. Derrac, S. García, D. Molina, and F. Herrera, "A practical tutorial on the use of nonparametric statistical tests as a methodology for comparing evolutionary and swarm intelligence algorithms," *Swarm Evol. Comput.*, vol. 1, no. 1, pp. 3–18, Mar. 2011.

LUIS ERNESTO VALENCIA-SEGURA received the B.S. degree in electronics and the M.Sc. degree in electronics sciences (automation) from Benemérita Universidad Autónoma de Puebla (BUAP), Puebla, in 2015 and 2016, respectively. He is currently pursuing the Ph.D. degree in robotic and mechatronic systems engineering with Unidad Profesional Interdisciplinaria en Ingeniería y Tecnologó as Avanzadas (UPIITA), Instituto Politécnico Nacional (IPN), Mexico City, Mexico. His current research interests include the design and implementation of bio-inspired metaheuristics for optimization and their application to engineering problems.

MIGUEL GABRIEL VILLARREAL-CERVANTES (Member, IEEE) received the B.S. degree in electronics engineering from the Technological Institute of Veracruz, Veracruz, Mexico, in 2003, and the M.Sc. and Ph.D. degrees in electrical engineering from the Center for Research and Advanced Studies (CINVESTAV), Mexico City, Mexico, in 2005 and 2010, respectively. He also studied a technical career in computer systems with the Centro de Computación Profesional de Golfo S. C., from 1998 to 2000. He was the Head of the Mechatronic Section, Centro de Innovación y Desarrollo Tecnológico en Cómputo, Instituto Politécnico Nacional (CIDETEC-IPN), Mexico City; and Expert Network on Robotics and Mechatronics, IPN (ENRM-IPN). He is currently a Full Professor with the Postgraduate Department, CIDETEC-IPN. His current research interests include mechatronic design based on optimization (mono and multiobjective optimization), bio-inspired meta-heuristics in the optimal mechatronic designs, the optimal tuning for the mechatronic system control based on meta-heuristic algorithms (offline and online strategies), and robotics. He is a member of the National System of Researchers in Mexico and ENRM-IPN.

LEONEL GERMÁN CORONA-RAMÍREZ received the degree in electromechanical engineering from the Technological Institute of Apizaco, the master's degree in electrical engineering from the Center for Research and Advanced Studies, National Polytechnic Institute (CINVESTAV-IPN), and the Ph.D. degree in mechanical engineering in the robotics line from the Higher School of Engineering and Mechanics, National Polytechnic Institute (ESIME-IPN). He is currently a Research Professor of mechatronics with the Department of Advanced Technologies, Interdisciplinary Professional Unit in Engineering and Advanced Technologies, National Polytechnic Institute (UPIITA-IPN). Between his developed works it is possible to emphasize the following: the author of books within the area of robotics, digital electronics, and sensors and actuators; the Founder of the UPIITA-IPN Robotics Association; the publication of articles in various magazines and congresses; and the director of thesis in undergraduate and postgraduate studies.

FRANCISCO CUENCA-JIMÉNEZ received the B.S. degree in mechanical engineering from the Technological Institute of Oaxaca, in 1993, and the M.S. and Ph.D. degrees in mechanical engineering from the National Autonomous University of Mexico (UNAM), in 1996 and 2008, respectively. He has been a Professor of mechanical engineering with the Faculty of Engineering, UNAM, since 1995. His research interests include kinematic and dynamic multibody modeling and mechanism synthesis.

JOSÉ SAÚL MUÑZ-REINA received the B.S. degree in bionic engineering from Unidad Profesional Interdisciplinaria en Ingeniería y Tecnologí as Avanzadas del, Instituto Politécnico Nacional (UPIITA-IPN), Mexico City, Mexico, in 2015, and the M.Sc. degree in computer technology from the Centro de Innovación y Desarrollo Tecnològico en Cómputo, Instituto Politécnico Nacional (CIDETEC-IPN), Mexico City, in 2018, where he is currently pursuing the Ph.D. degree in robotic and mechatronic systems engineering. His research interest includes the optimal design of mechatronic systems.